Chitosan/Hydroxyapatite Scaffolds with P28 as a Promising Osteoinductive Scaffold for Bone Healing Applications

Farah Alwani Azaman [1] , **Florence Daubiné** [2], **Amélie Lebatard** [2], **Margaret E. Brennan Fournet** [1]
and Declan M. Devine [1,*]

1   PRISM Research Institute, Technological University of the Shannon, Midlands Midwest,
    Athlone Main Campus, N37 HD68 Athlone, Ireland
2   Atlantic Bone Screen, 44800 Saint-Herblain, France
*   Correspondence: ddevine@ait.ie

Abstract: Despite bone's inherent ability to heal, large bone defects remain a major clinical concern. This study proposes an off-the-shelf treatment combining chitosan/hydroxyapatite (CS/HAp) scaffolds, covalently linked with either bone morphogenetic protein-2 (BMP-2) or its related peptide P28 via a UV crosslinking process. Although covalently binding the growth factors was reported as a great alternative to the conventionally physical adsorption and encapsulation methods, this method presents the risk of altering the molecular activity and interaction of the growth factors. Therefore, alkaline phosphatase (ALP) activity and alizarin red staining (ARS) with a quantitative cetylpyridinium chloride (CPC) assay were conducted to validate that our photo-crosslinking fabrication method did not interfere with the functionality of the growth factors. The ALP activity of C2C12 with 100 µg/mL P28 was found to be comparable to 0.5 µg/mL BMP-2 after two weeks, where 0.001 U/mL was recorded for both treatments. The C2C12 cultured with CS/HAp/BMP-2 and CS/HAp/P28 scaffolds also showed an increased ALP activity compared to the negative control. ARS-CPC assay presented the highest optical density in 0.3 µg/mL BMP-2 and 50 µg/mL P28, while the highest intensity of ARS was observed in C2C12 cultured with CS/HAp/BMP-2 and CS/HAp/P28 scaffolds compared to the negative controls. The osteoconductive capability of this delivery system was then investigated through a rat femoral condyle defect model, where the new bone mineral density and the bone volume increased for all CS/HAp scaffolds compared to the collagen sponge control treatment. The histological assessment showed a favourable bone regeneration efficacy of the CS/HAp/P28 compared to the CS/HAp/BMP-2 treatment, thus showing the use of CS/HAp scaffolds with P28 as a promising osteoinductive scaffold for bone healing applications.

Keywords: bone healing; scaffold; protein; peptide; osteoinduction; calcification; femoral condyle defects model

1. Introduction

Critical bone defects are caused by various factors, including high-impact trauma from falling or collisions, cancer, and bone diseases, which have been a global challenge to clinical orthopaedics for centuries [1–5]. While autologous treatment is favoured for its gold-standard features, it requires additional surgery and its limited supply demands the need for alternatives [6,7]. To date, substantial investigations have been carried out by tissue engineering researchers collaborating with orthopaedics and plastic surgeons to come up with off-the-shelf treatment alternatives for treating bone defects [8,9]. Researchers are investigating the use of available biomaterials to produce biodegradable bone substitutes that have been the current go-to alternatives since it is a critical factor in the success of new tissue turnover [10,11]. This biodegradable biomaterial comprises synthetic biodegradable polymers, such as poly lactic-co-glycolic acid (PLGA), and naturally occurring polymers, such as chitosan, silk fibroin and collagen, as well as inorganics such as hydroxyapatite, tri-calcium phosphate and antimicrobial fluorapatite [12–14].

Chitosan has been utilised in numerous research articles as a bone substitute for materials due to its biocompatible and biodegradable properties and the ability to promote cell attachment and proliferation, while it costs less compared to the other materials [15,16]. It has also been approved by the Food and Drug Administration (FDA) as a Generally Recognised as Safe (GRAS) biomaterial to be used for biomedical applications [17–20]. In addition, bone regeneration research has directed a significant application of chitosan composite in the formulation since it gives minimal foreign body reactions, has intrinsic antibacterial nature and can also be constructed into various geometries and forms for tuning the porosity, osteoinduction and osteoconduction properties [21]. Chitosan can also mimic the extracellular matrix (ECM) due to its similar structure to proteoglycans, which has led researchers to utilise it for tissue engineering [22–25]. However, owing to its low solubility property, chitosan is often combined with other biomaterials, such as hydroxyapatite, to improve its solubility as well as to enhance the mechanical properties and provide bioactive features to the bone scaffold [14,26–28]. Moreover, despite their known osteoconductive properties, CS and HAp require the incorporation of growth factors to enhance the osteoinductive feature of the scaffolds, where osteodifferentiation of the stem cells into osteoblasts is promoted [29,30].

Consequently, a promising acellular strategy that centres on developing scaffolds incorporating osteogenic factors was employed. This plan combines biology and engineering principles to create viable substitutes to restore and maintain the function of human (bone) tissue, involving covalent bonding of the growth factors to the composite vehicle through UV crosslinking. This method is one of the alternatives to overcome the limitations of surface adsorption and physical encapsulation methods, such as the unspecific affinity between the protein and carrier and the rapid uncontrolled release, respectively. This preferred alternative was reported to be efficient in yielding a thorough, stable and extended release instead [14,31,32] due to the controllable concentrations and the directed peptide conformations. In addition, covalently bound peptides were declared to have higher stability and specificity in terms of controlling the intended folding, thus allowing signalling and binding domains to be available for cellular interactions [33].

This project was aimed at fabricating a biodegradable scaffold that will release growth factors while degrading in a gradational way for an expected period to be replaced by a newly formed bone tissue from the bonded cells (osteotransduction) and then be secreted from the body naturally after it completes its function [34]. Previously, the FDA had approved a clinically relevant protein, the recombinant human bone morphogenetic protein-2 (rhBMP-2), with a collagen carrier called INFUSE® to induce new bone tissue following the implantation [35]. However, due to the ectopic bone formation resulting from the implantation, a P28 peptide derived from the knuckle epitope of BMP-2 was then examined as an alternative [3,36,37]. This P28 peptide was postulated to present a comparable osteoinductive performance to its protein of origin since it was previously found to be a potential substitute for the full-length rhBMP-2 in inducing new bone-cell formation due to its high performance with greater control over cellular interactions and a cost-effective alternative to BMP-2 [33,38,39].

C2C12 myoblast cell line, which has a low baseline ALP activity, normally regulates the osteoinduction process through the growth factor incorporation, typically BMP-2 (MW: 26 kDa), by altering the differentiation pathway of the myoblasts towards an osteoblastic lineage [40,41]. An upregulation in ALP activity induced by BMP-2 indicates the bioactivity of these osteogenic factors [42,43]. However, to our knowledge, no previous study has reported the C2C12 differentiation profile upon the osteogenic induction by P28 peptide (MW: 3091.2 Da) with the sequence of $S^{[PO4]}$ DDDDDDDKIPKASSVPTELSAISTLYL. Therefore, the C2C12 responses towards P28 treatments compared to BMP-2 on their own, or following the incorporation into the CS/HAp scaffolds in the cell testing, were systematically studied.

2. Materials and Methods

Chitosan (high MW), hydroxyapatite, ethanol $\geq$ 99.8% and Alizarin red S powder were obtained from Sigma Aldrich (Sigma Aldrich Ireland Limited, Co., Wicklow, Ireland). Sodium bicarbonate 99.5% was purchased from Acros Organics (Fisher Scientific UK Ltd., Loughborough, UK), poly(ethylene glycol) (600) dimethacrylate was obtained from Polysciences Inc. (Polysciences Europe GmbH, Eppelheim, Germany) and benzophenone, 99% (A10739.30) was purchased from Alfa Aesar (Thermo Fisher Scientific, Kandel, Germany). Human/Murine/Rat BMP-2 (*E. coli*) was purchased from Peprotech (Peprotech House, London, UK), while the P28 peptide (>98% purity) was obtained from Pepmic (Pepmic Co., Ltd., Suzhou, China). Medtronic Infuse® rhBMP-2 was generously provided by Medtronic BioPharma, Watford, UK. The C2C12 murine myoblast cell line was purchased from the European Collection of Cell Cultures (ECACC). The alkaline phosphatase assay kit was purchased from Abcam (Abcam, The Netherlands). All materials were used as received.

2.1. Preparation of Chitosan/Hydroxyapatite Scaffolds with P28 or BMP-2 (CS/HAp, CS/HAp/P28 and CS/HAp/BMP-2) Using a UV Photocrosslinking

CS/HAp scaffold with 5 µL 0.1% (*w/v*) benzophenone was prepared according to the previous report by Azaman, F. et al. [14] prior to the growth factor and peptide incorporation. Briefly, 1.5 g of high molecular weight chitosan was dissolved in 12.5 mL 1% *v/v* acetic acid and left on the bench for an hour. The chitosan paste was then neutralised in 0.1 M sodium bicarbonate solution for 10 min before being pat-dried with filter paper. Subsequently, 100 µL of PEGDMA600 and 5 µL of 0.1% *w/v* benzophenone in ethanol were consecutively added and thoroughly mixed. HAp powder of a similar ratio to chitosan was then added to the paste and mixed thoroughly.

The BMP-2 and P28 peptide powder were reconstituted in ultrapure water to provide 20 µg/mL and 5000 mg/mL solutions, respectively. Then, either 5 µL of the BMP-2 solution or P28 was injected into each scaffold, making CS/HAp/100 ng BMP-2 and CS/HAp/25 µg P28 scaffolds. Samples were then UV-cured for 10 min and flipped over mid-curing. Following the UV curing, all scaffolds were kept in a sterile container and frozen at −20 °C until they were ready to use. CS/HAp control scaffolds without growth factors were made in the same manner.

For the in vivo test, CS/HAp scaffolds were made as outlined above. However, 2 mg/mL rhBMP-2 and 5 mg/mL P28 were prepared before injecting 5 µL of the solutions into scaffolds prior to UV crosslinking to make CS/HAp/10 µg rhBMP-2 and CS/HAp/25 µg P28, respectively.

All CS/HAp scaffolds were sterilised using a bench-scale Pulsed-UV chamber (Samtech Pulsed UV system, Samtech Ltd., Glasgow, Scotland). A low-pressure (60 kPa) flash lamp containing xenon gas (Heraeus Noblelight XAP type NL4006 series encased in a clear UV transparent quartz tube) was connected to this chamber. This flash lamp generated a high-intensity broad-spectrum polychromatic pulsed light beam between 200–1100 nm [44]. The voltage was set to 800 V, and the pulse rate was one pulse/second, corresponding to 90 UV pulses of 800 V.

2.2. Fourier-Transform Infrared Spectroscopy

An attenuated total reflectance (ATR) Fourier-transform infrared (FTIR) spectroscopy was utilised to characterise the scaffolds (Perkin-Elmer Spectrum One FTIR spectrometer fitted with a universal ATR sampling accessory). A spectral range of 4000–650 cm^{-1} and four scans per sample cycle were carried out, with a resolution of 0.5 cm^{-1} at room temperature. All samples were dried in a vacuum oven at 37 °C and 70 mbar prior to the tests to avoid the broad water peak from shadowing the significant signature peaks of the materials. All spectra obtained were analysed following the tests to observe the linkage formed within all the formulations.

2.3. In Vitro Release Kinetics of BMP-2 and P28

BMP-2 and P28 incorporated scaffolds, and the empty control scaffolds (CS/HAp/BMP-2, CS/HAp/P28 and CS/HAp) were defrosted to room temperature on the bench for ca. five minutes prior to use. All scaffold samples used in this study had a thickness of 3 mm and 5 mm in diameter. The samples were separately placed in 2 mL Eppendorfs and filled with 200 μL of ultrapure water. Three scaffolds were used per formulation. The scaffolds were then incubated at 37 °C in a 120 rpm incubator shaker (Innova 4000, New Brunswick Scientific) for the following time points: 1, 6, 24, 48, 72, 192, 264 and 336 h to release the covalently-bonded growth factors over these 14 days. Aliquots of 150 μL were collected from each scaffold formulation at each time point and stored in 200 μL tubes. Aliquots were frozen at −20 °C until testing ($n = 3$). The tubes were then refreshed with the same 150 μL of ultrapure water.

Initially, both BMP-2 and P28-released samples were detected and analysed using a High-Performance Liquid Chromatography (HPLC) system (Waters Alliance 2965 Separations Module, Waters Ges.m.b.H., Vienna, Austria) fitted with Waters 2487 Dual Wavelength Absorbance Detector. However, issues related to the high affinity of the API towards the stainless-steel system were encountered, despite a number of troubleshooting executed to overcome these biocompatibility issues. Therefore, the amount of P28 released was quantified by using a UV-1280 UV Spectrometer (Shimadzu, Torrance, CA, USA) at 220 nm. The serial standards of P28 peptide were prepared at dilution factors of 1:20, 1:40, 1:80, 1:160, 1:320 and 1:640. The percentage of the released P28 peptide from the scaffolds was calculated using the equation from the standard curve.

(i)   Analyte concentration (μg/mL) = Concentration from equation × dilution factor.
(ii)   Mass of analyte (μg) = Analyte concentration × volume of samples.
(iii)   Percentage of analyte (%) = Mass of analyte ÷ Initial mass of P28 × 100.

However, BMP-2 samples were unable to be analysed using this system since their concentrations fell below the detection limit of the UV spectrophotometer.

2.4. Alkaline Phosphatase Assay

An alkaline phosphatase (ALP) assay was conducted to assess the efficacy of the protein and peptide incorporated into the CS/HAp scaffolds using an ALP test kit purchased from Abcam (Abcam Plc., Cambridge, UK) and used as instructed. C2C12 cells were seeded in a 24-well plate at a density of 5×10^4 cells per well and incubated for six hours before the treatment with BMP-2 (30, 300, 500 and 1000 ng/mL), P28 peptides (10, 50, 100 and 200 μg/mL), as well as the GF-infused CS/HAp scaffolds. Untreated cells and cells with the nude CS/HAp were set as the negative control.

All cells proliferated from each treatment were harvested and lysed at days four, seven and 14. The cells were placed into a microtube with 50 μL of assay buffer and lysed using a vortex for 20 s. After which they were kept on ice for ten minutes to break the cell membrane. Subsequently, the cell lysates were centrifuged at 4 °C and 10,000 rpm for 15 min in a cold microcentrifuge to remove any insoluble material. The supernatant was collected and kept in 0.2 mL PCR tubes.

ALP assay was conducted using the prepared C2C12 lysates. The samples were adjusted to 80 μL/well with the assay buffer. Subsequently, 50 μL of 5 mM ρ-nitrophenol phosphate (ρNPP) solution was added to each well containing the sample. Then, 10 μL ALP enzyme was added to each ρNPP standard well and mixed by pipetting up and down. The plate was incubated at 25 °C for 60 min and protected from light by wrapping the well plate with aluminium foil. The enzyme converted the ρNPP substrate to an equal amount of coloured ρ-nitrophenol (ρNP). After 60 min of incubation, the reaction in the sample and standard wells were deactivated by adding a 20 μL stop solution provided into each well. Finally, the 96-well plate was pre-shaken for ten seconds, and the output was measured at an optical density of 405 nm on a microplate reader ($n = 3$).

The ALP activity was calculated with respect to the ρNPP standard curve using the following formula:

$$\text{ALP activity} \left(\frac{\text{Unit}}{\text{mL}} \right) = \left(\frac{\text{B}}{\Delta \text{T} \times \text{V}} \right) \times \text{D}$$

where:

B = ρNP concentration from the equation (μmol)
ΔT = reaction time (min)
V = Original sample volume added into the reaction well (mL)
D = Sample dilution factor

Following the completion of this ALP assay in evaluating the best scaffold bioactivity performance, the work progressed to the alizarin red staining to further validate the osteogenic capacity of the developed scaffolds.

2.5. Alizarin Red Staining and Cetylpyridinium Chloride Assay

C2C12 myoblasts were seeded in 24-well plates at a density of 5×10^4 in 500 μL growth media per well and left to reach 80–90% confluency (approximately two days). The cells were refreshed with new growth media and treated with BMP-2 and P28 peptide standards as well as the scaffolds for four different time points; days 7, 14, 21 and 28. ThinCert™ transwells with a 0.4 μm pore diameter, compatible with 24-well plates were utilised in the test using scaffolds.

Alizarin red staining (ARS) procedures were conducted at each specified time point. All wells containing the cells were rinsed with PBS twice before the fixation using 300 μL of 10% formalin for 20 min. The wells were washed with PBS thrice after the fixation to remove the excess formalin solution. The wells were then stained with 300 μL of 2% ARS solution in water for another 20 min. The ARS solution was freshly prepared before each assay, with the pH of the ARS solution adjusted to 4.2 using 0.5% ammonium hydroxide. After 20 min, all wells were washed with 1 mL distilled water approximately five times or until no unbound ARS staining solution was left in each well. The stained C2C12 cells were left to air dry before capturing the images using Olympus CKX41 inverted microscope.

Subsequently, the cells were de-stained with 10% cetylpyridinium chloride (CPC) [45] to quantify the mineralisation exposed to the ARS stain, where 1 mL of CPC was added into each of the wells with dried ARS stain and incubated in 37 °C for 1 h. The dissolved stain was then spectrometrically analysed using the plate reader at 540 nm, pre-shake for ten seconds.

2.6. Femoral Defect Induction and Implantation

In vivo assessment of the scaffold was carried out through implantation in femoral condyle defects of three months old Sprague Dawley rats (*Rattus norvegicus*). This bilateral model was authorised by the local Ethical Committee and the French Ministry for Education and Research (agreement number: APAFIS#1437). The model applied for this study was in line with the European Directive 2010/63/UE.

Three formulations of scaffolds were fabricated for in vivo implantation procedures, with two additional samples as the positive control. The scaffolds fabricated off-the-shelves were CS/HAp, CS/HAp/10 μg Medtronic Infuse® rhBMP-2 (Medtronic BioPharma, Watford, UK) and CS/HAp/25 μg P28. Two additional samples were freshly prepared on the day of the implantation before the surgery: i.e., nude collagen sponges and collagen sponges infused with 10 μg of rhBMP-2 (Infuse®). Twelve SD rats were involved in this work (24 implantation sites).

The animals were acclimatised for a minimum of seven days and housed in adapted installations (air-conditioned rooms with a temperature of 22 ± 3 °C and a 50–60% humidity level). The artificial day/night light cycle was set to 12 h of light and 12 h of darkness. All animals had free access to water and were fed ad libitum with commercial chow daily. Cages were cleaned and changed weekly to prevent any unwanted infections at the surgical wound of the rats and their health generally. The general state of the animals was monitored daily.

The scaffold implantation was conducted using an aseptic technique. The operation comprised 3 mm round defects on both the right and left femoral condyles of animal models, which were adapted and modified from work carried out by Klein et al. and Mohiuddin et al. [5,46]. All instruments and apparatus were set up in a cleanroom.

Mixtures of oxygen/isoflurane (oxygen (0.4 L/min)/Isofluorane (1.5–2%)) were given as anaesthesia 15 min before the procedures and maintained throughout the surgery. The animals were maintained hydrated by a saline solution injection and eye gel application. A heating pad was installed throughout the procedures to maintain the temperature of the animals. The flanks of the animals were shaved by using an electronic hair shaver. Chlorhexidine was applied to the exposed skin, followed by povidone-iodine in an outward circular motion. A local anaesthesia injection (lidocaine and buprenorphine) was administered prior to a firm incision on the skin into the muscle using a scalpel blade. The doses of all drugs were calculated based on animal weight which was measured just before the surgery using the formula below:

$$\text{Dosage (mL)} = \frac{\text{weight (kg)} \times \text{dose}\left(\frac{\text{mg}}{\text{kg}}\right)}{\text{concentration}\left(\frac{\text{mg}}{\text{mL}}\right)}$$

The muscle mass was then dissected, exposing the bone surface of the femoral condyle. A commercial micro drill with a 3 mm bur was utilised to make a 3 mm-size defect with saline irrigation. Subsequently, a piece of the chitosan-based scaffolds was quickly inserted into the defect in a randomised manner, followed by suturing the muscle and skin with an absorbable suture consecutively and followed by a surgical staple. The animals were then returned to the cage. The post-operative health condition, weight, wound healing and behaviour of the animals were monitored frequently for eight weeks until the euthanasia procedure using cervical dislocation under anaesthesia.

2.6.1. Post-Operative Monitoring

The general post-operative conditions of the animals were monitored daily, and deeper monitoring in terms of body weight was recorded every two days in the early weeks post-implantation and every four days towards the end of the experiment. These monitoring procedures were carried out to observe whether the animals had reached the endpoints below, where euthanasia is mandated:

- Weight loss > 20% of the mean weight of rats;
- Severe lameness;
- Diarrhoea/blood in faecal material;
- Circling phenomenon;
- Severe necrosis at the implantation site;
- Persistent self-induced trauma five days after analgesic treatment as well as local and general treatment;
- Abnormal behaviour even in the presence of appropriate treatment (e.g., sign of pain even under analgesia).

2.6.2. Fluorescent Bone Labelling for Dynamic Bone Formation

In order to highlight the calcification front, all rats were subcutaneously injected with double-fluorochrome labelling; calcein and xylenol, ten and four days, respectively, prior to sacrifice [47]. These fluorescent labels were able to bond to the calcium from when the mineralisation process occurred. Calcein injection (10 mg/kg) was prepared by dissolving 0.1 g of calcein powder in a 2% sodium bicarbonate solution under sterile conditions [48]. The solvent was first prepared by dissolving 0.05 g sodium bicarbonate powder in 10 mL of 0.9% sterile saline solution, making the concentration 10 mg/mL. Xylenol injection (90 mg/kg) was prepared by weighing 0.2 g sodium bicarbonate and dissolved in 10 mL of 0.9% sterile saline solution under sterile conditions. The solvent was poured into 1 g of xylenol orange tetrasodium salt and shaken until dissolved.

Following euthanasia, the femurs of the rats were collected by incising the muscle until reaching the femoral head, and the ligaments holding the femoral head and the condyles were cut. The surrounding muscle was removed as much as possible. The femurs were then fixed in 10% neutral buffered formalin and cut using a hard tissue cutter, obtaining the implanted femoral condyles.

2.7. Micro-CT Analysis of Femoral Condyle Defects

Calibration phantom scans for bone mineral density (BMD) measurements were run using calcium hydroxyapatite samples of known BMD by utilising the same conditions as the test samples. The images were analysed using SkyScan Image Analyses Software and Bruker CTAn Micro-CT Software (CTAn software v.1.18) to assess two bone morphology parameters: bone mineral density (BMD) (g·cm^{-3}) and bone volume fraction (BV/TV) (%), where BV is the bone volume, and TV is the total volume.

2.8. Histological Processing, Staining and Analysis

After fixation process, femoral condyles were dehydrated in increasing concentrations of ethanol solutions and cleared in xylene. Then, the samples were embedded in a resin specifically developed for mineralised tissues (Technovit 9100, Kulzer GnmH, Hanau, Germany) at -11 °C. Serial longitudinal sections of 3–7 µm thickness were performed at the defect level to obtain sagittal view of the defect using the sawing microtome.

Sections were stretched on slides by immersion in an alcohol solution and covered with polyethylene films to dry. After drying, sections were deplasticised and the following staining were performed: Hematoxylin-Eosin (HE), Von Kossa (VK) and Tartrate-Resistant Acid Phosphatase (TRAP). Non-stained slides were also prepared for the fluorochrome labelling analysis.

2.9. Statistical Analysis

All statistical analysis in this document was performed using the Minitab software. Firstly, a descriptive statistic was performed to evaluate the mean and standard deviation between the samples. The significance between the two data groups was then tested using a student *t*-test. Subsequently, a one-way ANOVA was utilised to compare three or more parametric data groups, followed by a Tukey's test to assess the significant changes in the data. A Kruskal–Wallis test was conducted for non-parametric tests. Significance was achieved with data exhibiting a *p*-value less than 0.05 ($p < 0.05$).

3. Results and Discussion

3.1. Scaffold Characterisation through a Fourier-Transform Infrared Spectroscopy

The chemical compositions of the fabricated scaffolds were analysed using FTIR. Chitosan characteristics could be observed through the saccharide C-O-C stretching at 1150, 1060 and 1020 cm^{-1} and the asymmetrical C-H stretch of –CH$_2$ at 2921 cm^{-1} [45,49], while HAp was commonly presented by the calcium phosphate regions at 1029, 1049, 1089, 980–1100 cm^{-1} and carbonate regions at 1670–1420, 1418, 1471 cm^{-1} [50–53]. In this work, the CS/HAp scaffold exhibited the asymmetrical C-H stretch of –CH$_2$ at 2871 cm^{-1} and the calcium phosphate regions at 1017, 1089, 1148 and 1049 cm^{-1}, corresponding to values presented in the literature.

Halloran et al. [54] identified BMP-2 through two different amide bands of the protein at 1664 and 1393 cm^{-1}, while Rosenberg et al. [35] observed the amide I at 1633 cm^{-1} and amide II at 1533 cm^{-1}. Interestingly, the BMP-2 and P28 in this work portrayed only the amide I band at 1636 cm^{-1} (Figure 1). This P28 profile was likely due to the protein of origin of the peptide, which was BMP-2, therefore it gave similar values [1,3,38].

While the concentration of BMP-2 in the mixture was low compared to the other constituents in the construct, there was an observed increase in the peak height at 1650 cm^{-1}, which could be caused by the incorporation of BMP-2. Similarly, there was a further in-

crease in the peak height following the incorporation of P28, which was added at a higher concentration compared to BMP-2.
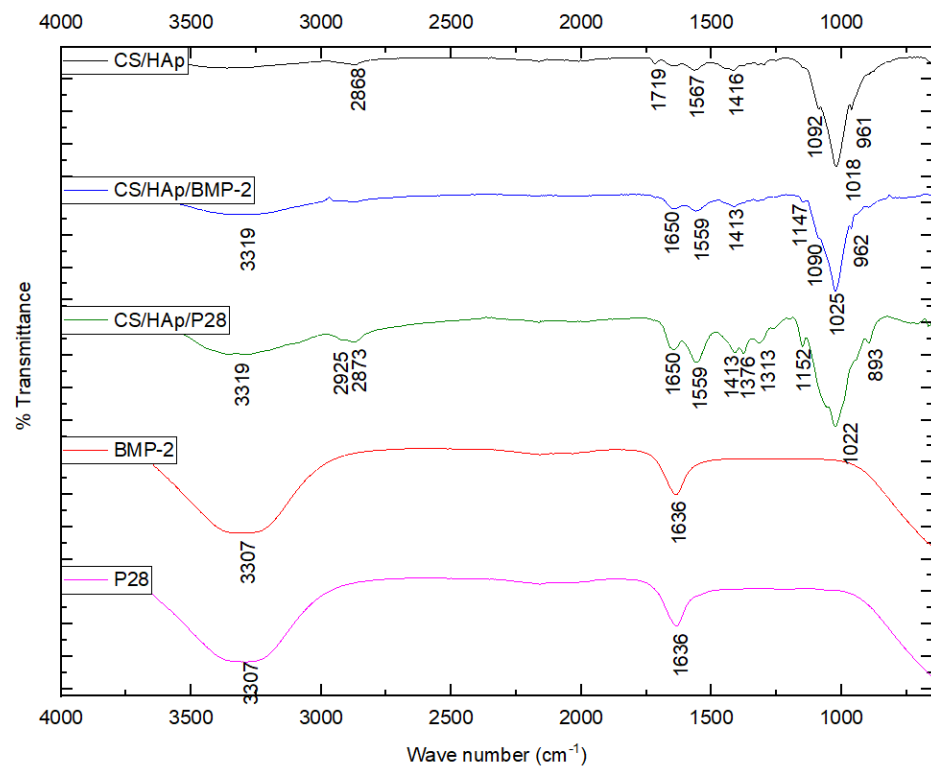

Figure 1. FTIR responses of the scaffolds, BMP-2 and P28, presenting the success of the covalent bonding through the increase in the peak height at 1650 cm^{-1}.

3.2. In Vitro Kinetic Release of P28

The cumulative release of the P28 peptide from CS/HAp scaffolds in ultrapure water was measured using a UV spectrometer (Figure 2). Initially, the API release was planned to be analysed using an HPLC system. Hence, ultrapure water was chosen to eliminate complexity in separation. However, there were difficulties in terms of protein/peptide high affinity towards the stainless-steel system, resulting in the inability to proceed with HPLC, and UV spectrometer was used as an alternative.

Within 48 h, 27.43 ± 0.18% of P28 incorporated in the scaffolds was released in a burst release manner, followed by a sustained release from 72 h until the end of the study at 14 days (2.84 ± 0.01 to 2.42 ± 0.01%). Cumulatively, 38.09 ± 0.2% of the total P28 was detected in 14 days, and therefore, it was postulated that ~95% P28 peptide would be released in five weeks, should the release rate remain consistent. This finding agreed with the bone healing timeframe, which usually takes about 6–8 weeks [11,14,55]. Consequently, this release profile obtained could validate the efficiency of our CS/HAp scaffolds to retain the P28 peptide within the composite and thus serve as the delivery vehicle for the peptide, thereby promoting new bone formation [38].

These results compare favourably to previous work carried out by Sun, T. et al. [1], who incorporated P28 peptide into a nanohydroxyapatite/collagen/poly (L-lactide) (nHAp/C/PLA) scaffold and recorded a sustained release over 14 days compared to P4 peptide and BMP-2. At 14 days, 72 ± 3% of P28 had been released compared to nearly 100% for P4 and BMP-2. This profile showed the better affinity of P28 towards nHAp/C/PLA scaffolds. The affinity of P28 to HAp-containing scaffolds may also explain the slow release observed in the current study. These findings emphasise that good P28 affinity towards the scaffolds is crucial in order to extend the release profile and thus enhance osteogenesis [56–58].
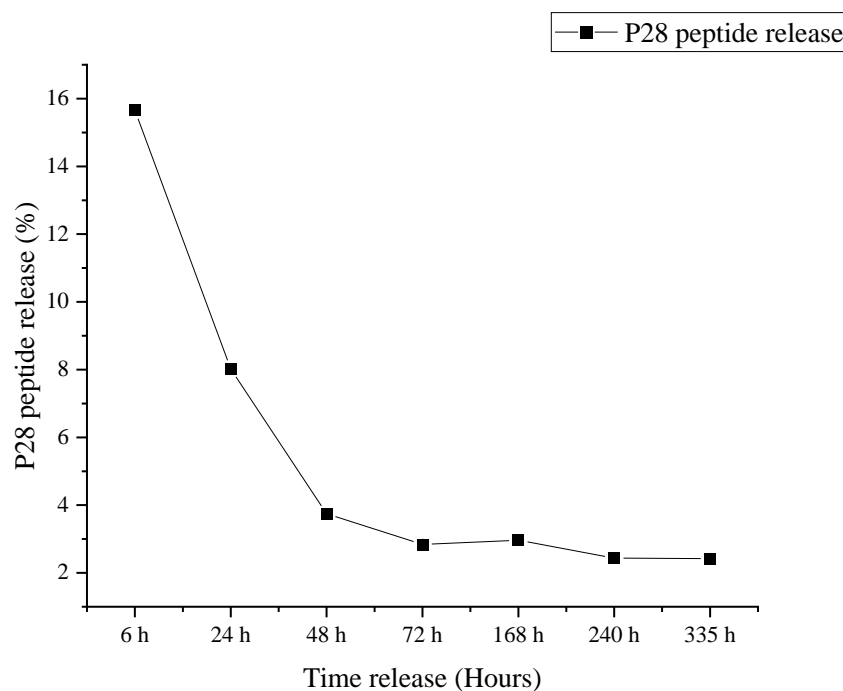
Figure 2. P28 release profile showing an initial burst release in the first 48 h, followed by a sustained release until 335 h (14 days).

3.3. C2C12 Mineralisation through Culture with P28 Peptide and BMP-2 Loaded Scaffolds Using Alkaline Phosphatase

C2C12 cells are myoblastic cells known to upregulate alkaline phosphatase (ALP) expression following exposure to BMP-2 [59]. It is hypothesised that as P28 is derived from, and has a similar structure to, BMP-2, it will also upregulate ALP expression following culture with C2C12 cells. Therefore, ALP assays for C2C12 were performed in the presence of various concentrations of both BMP-2 (0.1, 0.3, 0.5 and 1 µg/mL) and P28 (10, 50, 100 and 200 µg/mL), as well as post-treatments with scaffolds (CS/HAp, CS/HAp/BMP-2 and CS/HAp/P28) in complete DMEM + 10% FBS for 4, 7 and 14 days of cell culture (Figure 3).

A high background was observed in the negative control, which was the untreated cells over the 14 days ($p > 0.05$). For each BMP-2 concentration, a reduction in ALP activity was observed from day 4 to day 7 before an upregulation of ALP expression from day 7 to day 14 for the treated C2C12 cultures. The BMP-2 standard with 1 µg/mL concentration presented the highest ALP activity compared to the other BMP-2 concentrations for the given culture time ($p < 0.05$). Generally, the ALP response in the C2C12 treated with BMP-2 in this work was lower than ALP expression from C2C12 cells reported by Katagiri et al. [43], where 0.6 U/mL alkaline phosphatase activity was recorded after six days of incubation. The reason for the lower-than-expected mineralisation data could be the method used to lyse the cells, which in this case was a mechanical disruption method using a vortex, which may have been inefficient compared to the pulsed sonicating device recommended by the kit supplier but was not available in our laboratory. Nevertheless, the increase in ALP expression indicates the inhibition of the C2C12 myogenic cell lineage following the osteogenic treatments with BMP-2 [41].

Previously, researchers had studied the osteoinductivity of P28 peptide in the culture with MC3T3-E1 pre-osteoblasts phenotype [1,58]. To our knowledge, no study has investigated the application of P28 peptides in converting the differentiation pathway of C2C12 in bone healing treatments. Therefore, we used the same C2C12 culture system indicated for BMP-2 treatments, with cells cultured in various P28 peptide concentrations. Corresponding to the BMP-2 response, an initial reduction in the ALP activity was observed from day 4 to 7 before increasing on day 14. However, after 14 days of treatment,

the ALP response remained lower than on day 4 in all P28 concentrations, although no significant difference was recorded ($p > 0.05$). The potential of several peptides derived from the similar knuckle epitope of BMP-2, such as P28, to induce calcification in the murine multipotent mesenchymal (C3H10T1/2) cell line and upregulation of ALP activity have been reported [60]. P28 peptide scaffold's efficacy had also been investigated, where the positive ALP activity in the chitosan scaffold on the pre-osteoblast cell line, MC3T3-E1, was addressed [2]. In addition, a recent study reported the use of another five peptides derived from BMP-2 knuckle epitope named P1 to P5 peptides to investigate the binding affinity of these peptides to the bone morphogenetic protein receptor (BMPRII) in the C2C12 cell line and deduced the P5 peptide to present the highest binding affinity to BMPRII and thus has the potential to promote osteogenesis [61]. Therefore, the BMP-2-derived peptides, especially from the knuckle epitope of the protein structure, are indeed osteoinductive, thus reserving the P28 osteogenic potential to be further investigated.
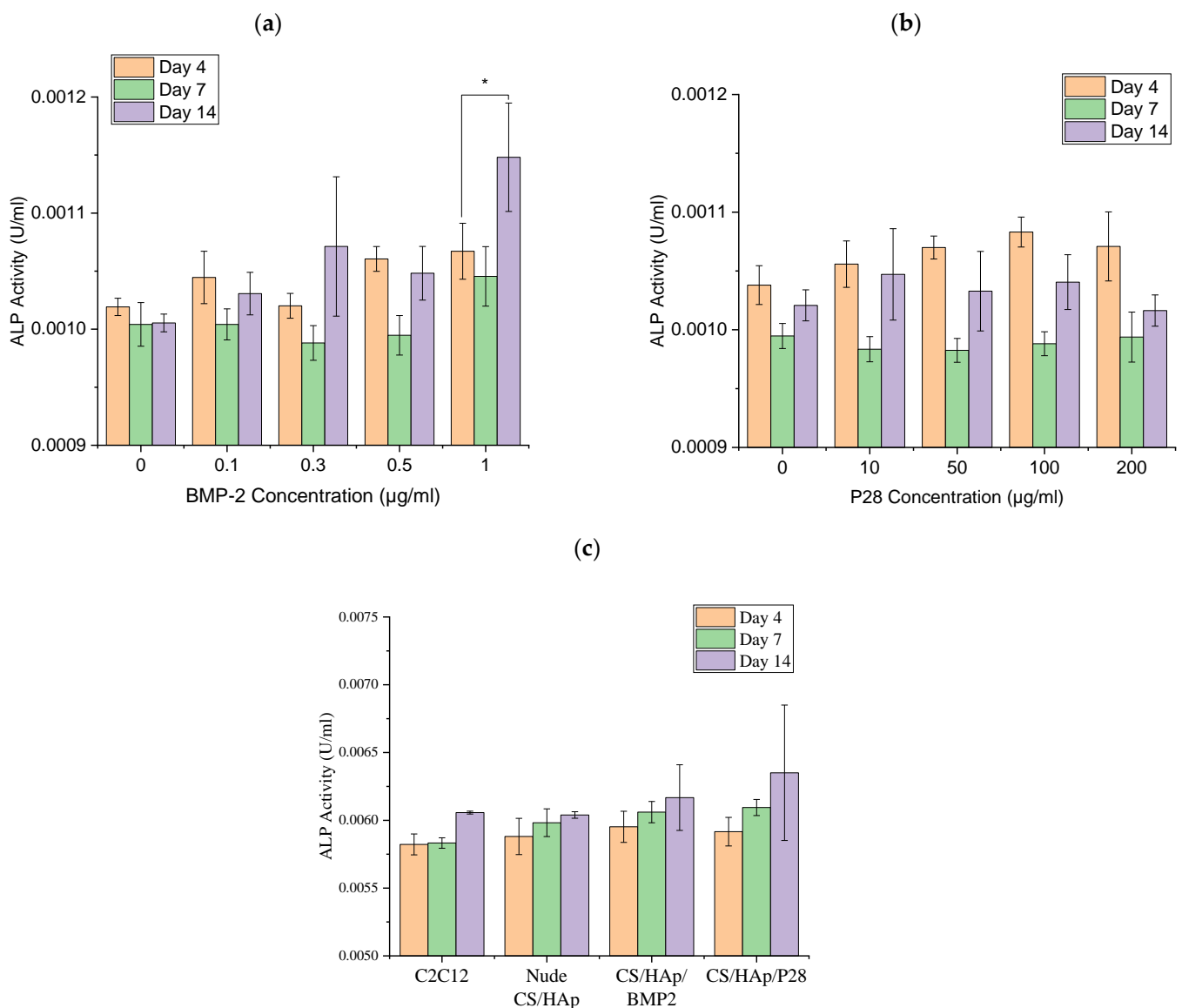

Figure 3. Alkaline phosphatase response of C2C12-treated with various concentrations of (**a**) BMP-2 and (**b**) P28 controls and (**c**) the CS/HAp scaffolds. An increased ALP response was observed in the culture with 1 µg/mL BMP-2 after 14 days, despite the high background control.

ALP activity of C2C12 cells was also assessed in the presence of BMP-2 and P28-incorporated scaffolds (CS/HAp, CS/HAp/BMP-2 and CS/HAp/P28) to investigate whether the growth factors remained bioactive following the crosslinking procedures employed in the preparation of the scaffold. A higher ALP response was recorded in the C2C12 culture with the CS/HAp, CS/HAp/BMP-2 and CS/HAp/P28 scaffolds compared to the culture with the growth factor standards presented previously. However, only day 7 of the culture showed a significant difference between the negative controls (C2C12 only and nude CS/HAp compared to CS/HAp/BMP-2 and CS/HAp/P28 ($p < 0.05$)), where an increased ALP activity was recorded for the growth factors incorporated scaffolds. In contrast, no significant difference was seen in the ALP activity in all samples on day 4 and day 14 of treatment. These results might be due to insufficient scaffold degradation or the small concentrations of both BMP-2 and P28 used in the scaffolds. However, the increase in ALP activity observed on day 7 illustrated the bioactivity of the growth factors following encapsulation. The ALP activity was lower than values reported in the literature following the incorporation of BMP-2 into scaffolds. However, in most, if not all cases, researchers utilised supplemented media, which was not used in this work. For example, Wu et al. [62] utilised 50 µg/mL ascorbic acid and 10 mM β-glycerol phosphate in their C2C12 cultured with or without 100 ng/mL BMP2, where they observed an increased differentiation following the treatments. In addition, similar components were supplemented as calcification medium (10 mM β-glycerophosphate and 50 µM ascorbic acid) in C2C12 cultured with midazolam and rhBMP-2, where mineralised nodules were observed after 10 days of treatment [41]. The supplemented media were postulated to increase the osteogenic induction further, thus enhancing ALP activity in the treatments containing the P28 standards and their associated scaffolds. The absence of these supplements in this current work might explain the lower ALP values recorded. However, the initial purpose of excluding the supplements was to eliminate any possible background responses and investigate the original osteoinductive response of our scaffold formulations without the external aid of an osteogenic medium.

A complementary investigation was attempted to validate the possible increased osteogenic response postulated earlier upon the change in the media composition. The FBS was decreased from 10% (growth medium (GM)) to 2% (differentiation medium (DM)) before treating the C2C12 cells with the scaffolds (Figure 4). The physical observations of the C2C12 culture in the different conditions showed the changes in the morphology of the cells after seven days in the culture using the DM and GM. It was observed that the myotubes were formed in the DM and GM culture without the scaffolds. When the scaffold was introduced, the structure of the cells changed with evidence of cuboidal structures observed in both media for all scaffold treatments, with the effect more pronounced in the GM cells [63,64]. Studies have previously shown that C2C12 cells maintained their tubular shape without the treatment of growth factors, while the cell morphology changed in the presence of lower FBS content (DM) and osteogenic factor conditions [43]. This morphology change observed indicates a change in the cell phenotype in response to the growth factor-loaded scaffolds. These results highlight that cell culture media selection is vital in differentiation experiments as it has the possibility to affect cellular behaviour and cell expression [65].

3.4. C2C12 Mineralisation through Culture with P28 Peptide and BMP-2 Loaded Scaffolds Using Alizarin Red Staining

Alizarin red staining (ARS) was utilised to stain calcium deposits or mineralised nodules due to osteogenic differentiation of C2C12 subsequent to the treatment of various BMP-2 and P28 peptide concentrations for 7, 14, 21 and 28 days, followed by a destaining step using cetylpyridinium chloride (CPC). The induction from BMP-2 and P28 growth factors will shift the differentiation pathway of the myoblasts towards an osteoblastic phenotype instead of the normal myotube pathway, thus causing mineralisation [66–69].
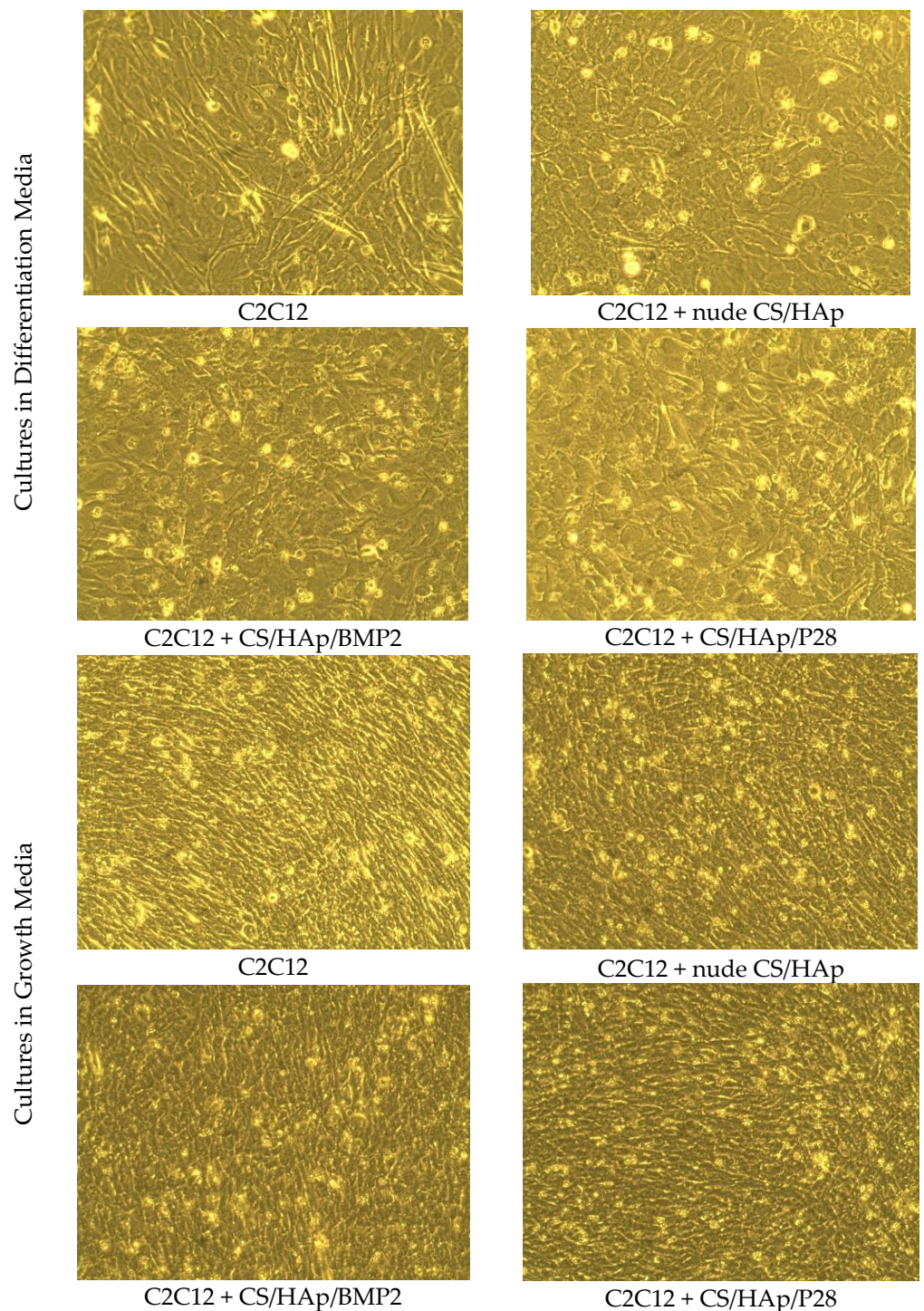
Figure 4. Morphological changes in C2C12 following cultured with the various scaffold formulations in differentiation media (magnification: 10×) and growth media (magnification: 4×). Cuboidal morphology can be observed in the culture with CS/HAp/BMP-2 and CS/HAp/P28 compared to the controls.

Positive ARS in C2C12 cultured with BMP-2 was observed, with an enhanced stain in the treatments with 0.5 and 1 µg/mL BMP-2 after four weeks (Figure 5a). In addition, there was an increased CPC response following the ARS in each of the BMP-2 concentrations over the four weeks of treatments ($p < 0.05$), where BMP-2 of 0.3 µg/mL gave the highest optical density of more than 0.5 after four weeks. Conversely, no significant difference was achieved for the negative control set over the four weeks ($p > 0.05$) (Figure 5b). The

response of the BMP-2-treated cells was higher compared to the controls, thus indicating increased mineralisation following the induction of the growth factors up to the fourth week. Positive results were also previously obtained through a study with the treatment of rhBMP-2 and fibroblast growth factor-2 (FGF-2) in C2C12 culture, where the 4 µg/mL of rhBMP-2 and 2 ng/mL FGF-2 showed the highest level of mineralisation after four weeks. However, the cells marked with ARS were not de-stained with CPC for quantitative values, hence presenting only qualitative observation [70].

Other interesting results were reported, testing the effects of rhBMP-2 in the calcification activity of C2C12 cultured with the osteogenic medium [41]. However, no appearance of the calcium nodules stained by ARS was observed in culture using an osteogenic medium with the presence of 0.5 µg/mL rhBMP-2 after ten days, whereas in the current study, calcium nodules were observed as early as seven days in the same concentration. This mineralisation shows that BMP-2 has the ability to shift the differentiation pathway of the C2C12, although the culture media used was not supplemented with any osteoinductive components such as the ascorbic acid and β-glycerophosphate that were used by the other studies [41,62,69,71]. Nevertheless, it was reported that the osteogenic medium would indeed enable the higher induction of mineral deposition of BMSCs in 14 days [72].

Subsequently, various P28 peptide concentrations were tested using ARS and CPC assay to assess the ability to induce C2C12 calcification. A positive ARS was visible from week two of the treatments and the staining intensity increased over the four weeks studied (Figure 5c). The CPC assay showed a significant difference in the staining intensity in each of the P28 concentrations over four weeks ($p < 0.05$) (Figure 5d). In addition, a significant difference was also obtained comparing the 0 and 10 µg/mL P28 to 50, 100 and 200 µg/mL P28 concentrations at week four ($p < 0.05$). This result indicated that P28 concentrations of 50 µg/mL and above can induce calcification in the C2C12 culture. This work is in alignment with the literature where ARS was conducted on the MC3T3-E1 pre-osteoblasts cultured with P28-infused scaffolds, where cells cultured with P28 scaffolds showed an increase in mineralisation compared to a negative control scaffold [58]. In addition, P28 was found to possess osteoinductivity similar to its protein of origin, BMP-2, which was further validated in vivo through the implantation of silicone/hydroxyapatite scaffold with P28 peptide (Si/HAp/P28) in the rat calvarial defects [2].

Complications with the use of high doses of growth factors have been widely reported [73–78]. As such, low-dose growth factor treatments (0.1 µg BMP-2 or 25µg P28) were used for ARS, carried out in the presence of the CS/HAp scaffolds UV-grafted with either (CS/HAp, CS/HAp/BMP-2 and CS/HAp/P28) for four weeks. The treated cells were stained with ARS (Figure 5e), which was followed by de-staining using CPC (Figure 5f). However, CPC results could not be measured until week 3 due to the sterility of the scaffolds causing contamination and leaving only one sample at week 4. Slightly positive ARS was observed in CS/HAp/BMP-2 and CS/HAp/P28 treatments in C2C12 compared to the cells without any scaffolds and the cells with nude CS/HAp. However, due to the low intensity of the ARS, the CPC assay shows no significant difference in all scaffold treatments. This low calcification might have been caused by the insufficient degradation of the scaffolds in vitro since the scaffolds were found to degrade after eight weeks, thus delaying the release of the growth factors in this mineralisation assay [14]. In addition, the low growth factor concentrations incorporated in the CS/HAp scaffolds might also have caused the low mineralisation seen in the cells. A previous study had reported that using 3 mg/mL P28 in the mineralised small intestinal submucosa (mSIS) scaffolds resulted in the highest mineralisations in the rat calvarial defects, compared to the negative control [56]. However, the P28 incorporation method used in this study was the absorption method which is known to lead to weak binding with the scaffold and to a burst release of ca. 10% of the P28 loading [56]. It is likely that the higher peptide concentrations used by Sun et al. led to a more rapid C2C12 response, thereby enhancing the cellular response.
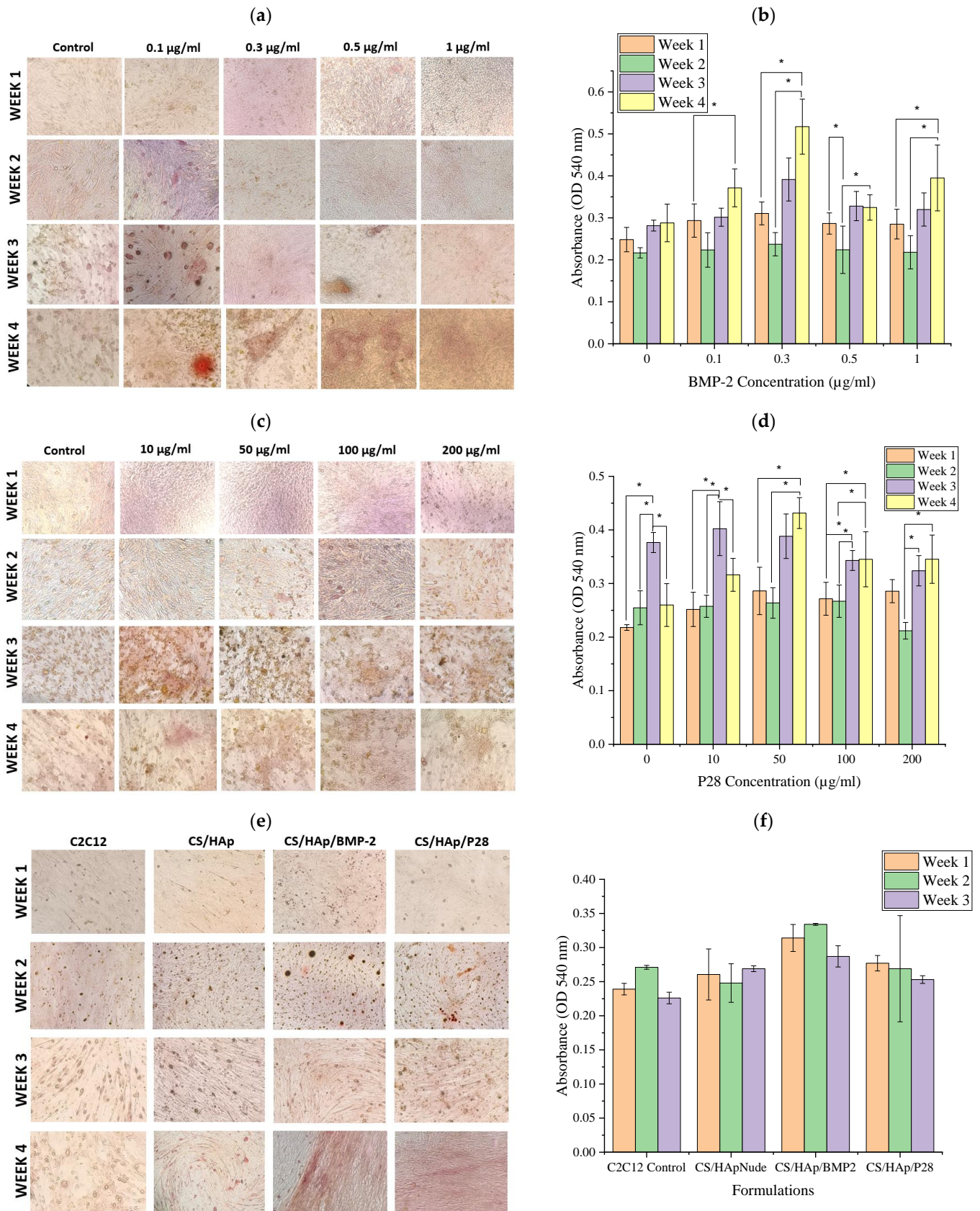
Figure 5. Alizarin red stained images and the destaining by CPC quantitation. (**a**) ARS of C2C12 treated with various concentrations of BMP-2. (**b**) CPC quantitation of the destained ARS of C2C12 treated with various concentrations of BMP-2. (**c**) ARS of C2C12 treated with various concentrations

of P28. (**d**) CPC quantitation of the destained ARS of C2C12 treated with various concentrations of P28. (**e**) ARS of C2C12 treated with various CS/HAp scaffolds. (**f**) CPC quantitation of the destained ARS of C2C12 treated with various CS/HAp scaffolds. Positive ARS was observed in week 4 following the treatments with BMP-2 and P28 as well as CS/HAp/BMP-2, CS/HAp/P28 compared to the controls. (* $p < 0.05$).

3.5. Post-Operative Evaluations of the Animals

The post-surgery recovery of the animals was examined in terms of pain, lameness, inflammation and growth rate, where the body weight of rats was compared relative to the initial weight before implantation [79,80]. In relation to the mean body weight curve per group, a slight decrease in body weight was noted just after the surgery. This bodyweight reduction could be explained by the lameness development that might decrease the animal's appetite, thus reducing the animal's capacity to catch food [81]. However, no intervention was needed since the rats did not reach the maximum admissible weight loss ($\leq$20%) [82]. In addition, it was observed that the mean body weight in all groups started to increase after day six, which was in line with the physiological increase seen with ageing, thus suggesting that neither the surgery nor the lameness affected animal metabolism [83]. The observed weight loss was similar to several studies reporting less than 10% weight loss post-operative, indicating a normal phenomenon [81,82].

3.6. Macroscopic Evaluation

Following euthanasia, the implanted femoral condyles defects were harvested, and local macroscopic evaluation was carried out. Traces of defects were still visible and appeared as small irregular bumps in condyles with the implanted CS/HAp scaffolds or collagen sponge alone (Figure 6). In contrast, they appeared as regular holes closed by transparent tissue in collagen sponge/rhBMP-2 condyles. The defects were visible in condyles implanted with CS/HAp scaffolds, whether the scaffold was conjugated with the growth factors or not, suggesting that the entry of the defect was not completely closed after two months of implantation. These visible defects might have been caused by the incomplete degradation of the chitosan-based scaffolds in vivo, although proven otherwise in vitro [7].

Observing the bone physiology, 71% of the femoral condyles in all types of implanted material were, surprisingly, twisted towards the defect side, compared to a normal femoral condyle (Figure 7). This bone torsion could have been caused by the presence of the scaffolds as foreign materials or the defect induction surgery causing a level of rotational instability upon ambulation from the press-fitted implant in the defects of the animals, which could not be confirmed due to the absence of an empty defect in this study [46]. However, a similar phenomenon was also seen in a study regarding an osteoarthritic joint remodelling, where slight gross morphological changes and deformations, such as twisted shapes in the temporomandibular joint of Sprague Dawley rats, were observed post-development of prosthetic unilateral anterior crossbite rodent model, which might have been caused by the modifications in deep zone cartilage [84,85].

3.7. Micro-CT Evaluation of the Femoral Defects Treated with the Scaffolds

Micro-computed tomography (µCT) scanning analyses were conducted on the implanted condyles following the harvest after eight weeks of implantation and the images were reconstructed to observe the new bone formation within the defects. In scaffold conditions (with or without rhBMP-2 or P28), the defect was mainly visible and delineated with bone tissue at the defect margin, while the entry of the defect remained empty. Femoral distortion was observed to be subsided to the side of the defect in all types of scaffolds, while no other bone lesions were observed (Figure 8). This architectural distortion observed in the remodeled bone could have been secondary to the various incidents of collapse, asymmetric growth and disturbed ossification process [86].
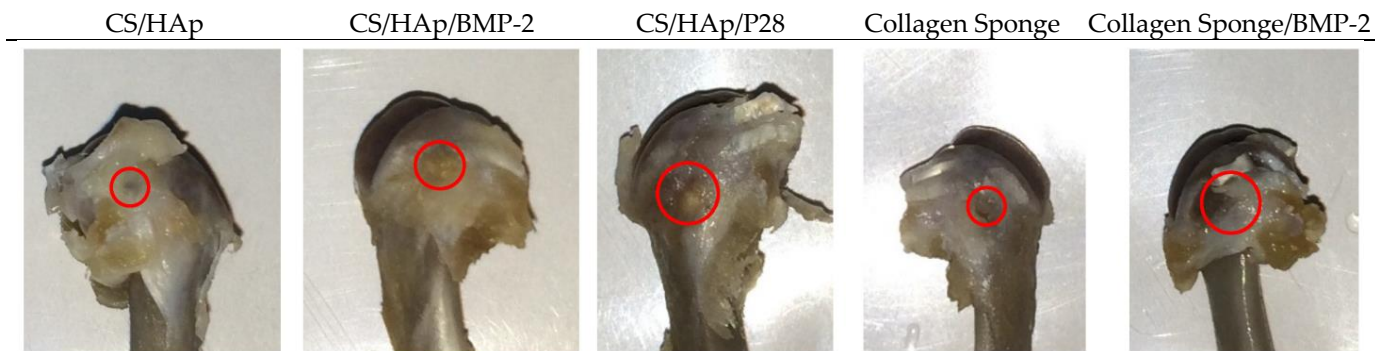
Figure 6. Defects visibility on the condyles after eight weeks (red circle). Traces of defects were still visible and appeared as small irregular bumps, especially in condyles with the implanted CS/HAp scaffolds.
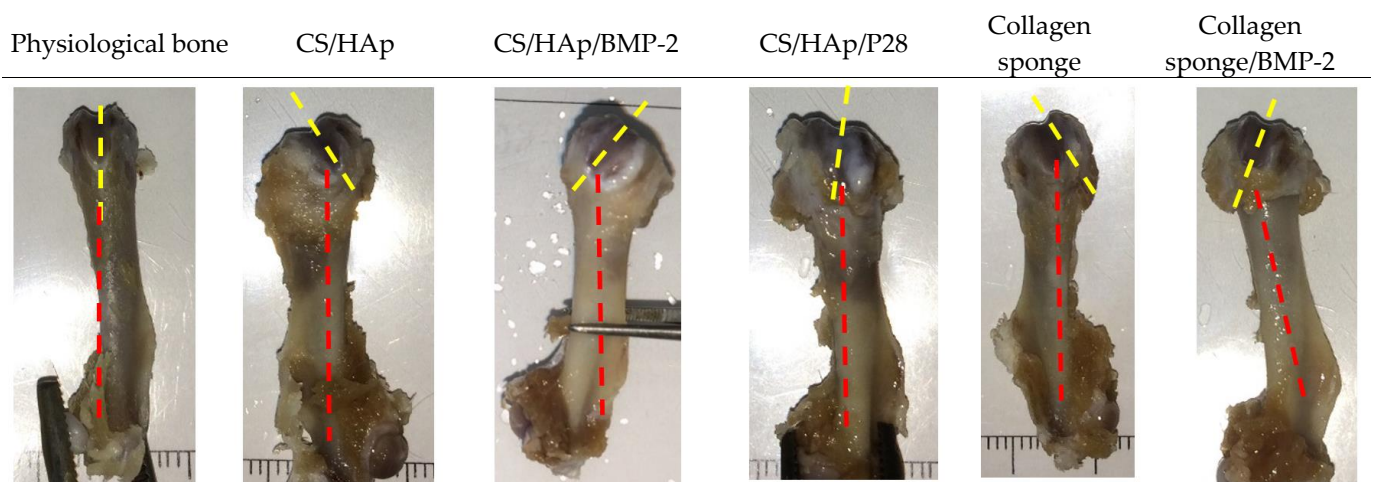

Figure 7. Representative images of twisted condyles comparisons between the implanted and physiological femoral condyle after eight weeks, showing that all groups experienced twisted condyle formation that might be caused by rotational instability from the defect induction and implantation. Annotations: Yellow broken lines = condyle axis; Red broken lines = femoral diaphysis axis.

In addition, mineralised areas inside the defect, and at the defect entrance, were observed. These mineralised areas may have corresponded to HAp residues (a mineralised cement) that could block the defect closure even after eight weeks. However, the mineralised areas may also have corresponded to newly formed bone islets, suggesting osteogenesis [87]. Conversely, the defect was almost not visible in condyles implanted with the collagen sponge (with or without rhBMP-2). Only a few traces of defect margin were still observed while the defect entrance was already closed. Moreover, the collagen sponge was not visible anymore. It was previously reported that the collagen sponge could be entirely resorbed in 28 days, thus showing that the bone healing was almost ended [88].

Quantitative Analysis of Micro-Computed Tomography Scanning

The bone volume fraction (BV/TV) and bone mineral density (BMD) (Figure 9) were measured, including both the entire defect and its margin (ROI 4 mm). The hydroxyapatite might have caused a higher bone volume fraction (BV/TV) and bone mineral density (BMD) in the presence of a chitosan-based scaffold compared to the collagen sponge, with a significant difference between collagen sponge/rhBMP-2 and CS/HAp/rhBMP-2 ($p < 0.05$) (there was an increase of 22% for BV/TV and 38% for BMD).
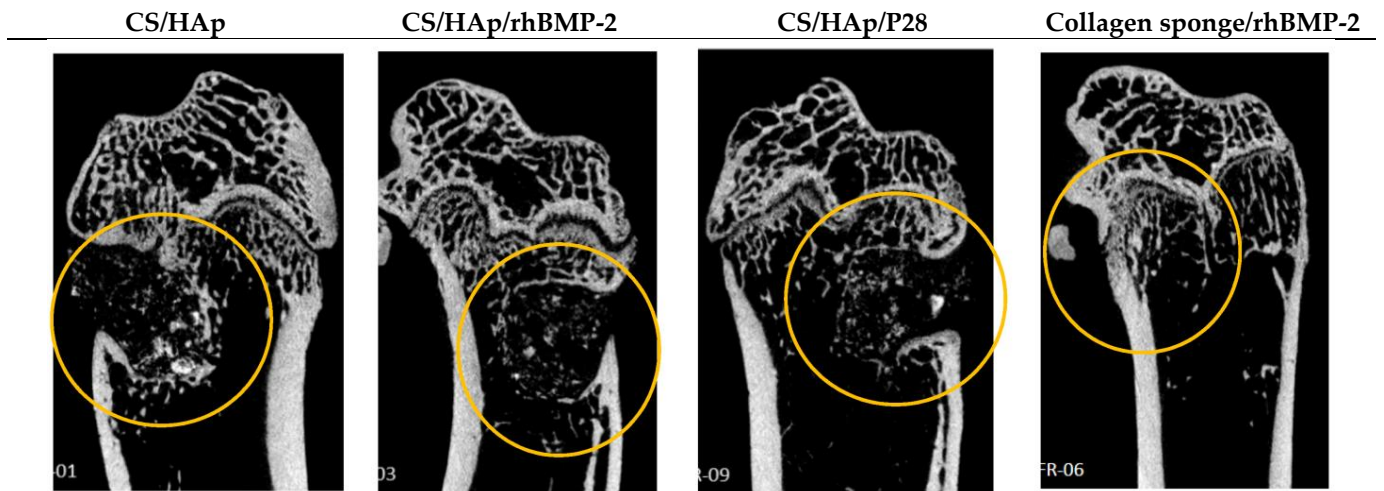
Figure 8. Representative coronal view images of the femoral condyle in CT scan per sample group after eight weeks of implantation. The condyle implanted with collagen sponge/rhBMP-2 is observed to reach the terminal healing process while traces of scaffolds were still present in CS/HAp scaffolds. However, CS/HAp/P28 gave better defect closure compared to CS/HAp and CS/HAp/rhBMP-2. (Annotation: Yellow circle = Implantation site).
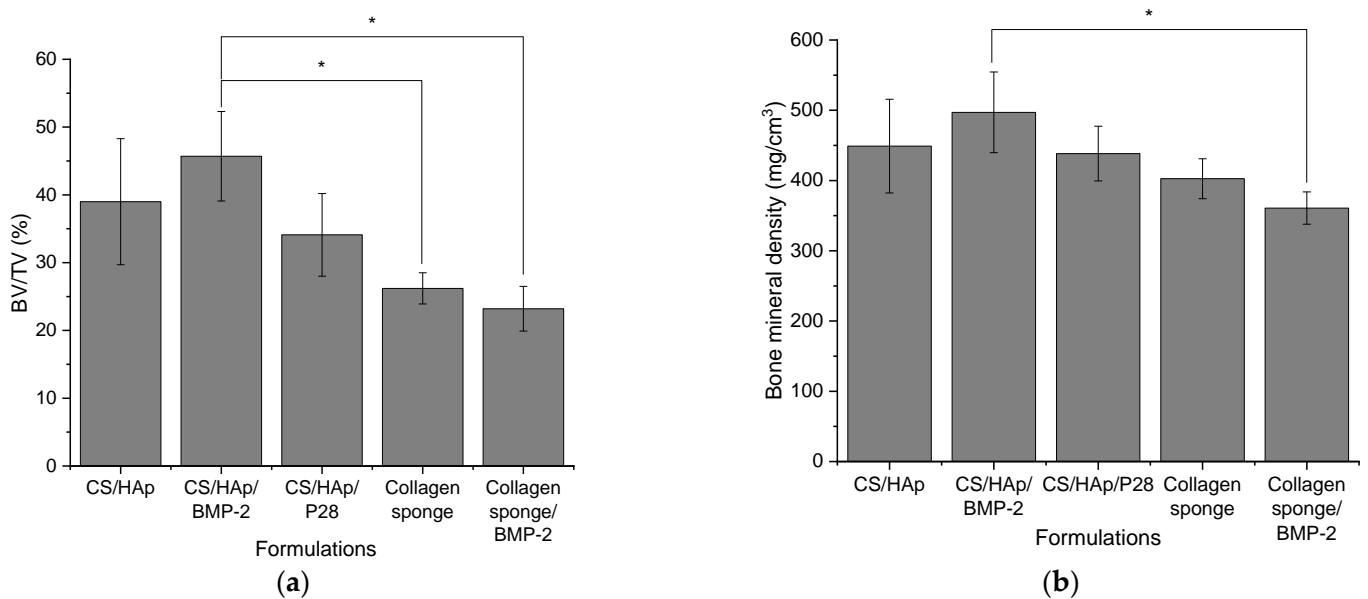

Figure 9. (**a**) Graph of mean volume fraction for each sample group in the entire defect and its margin after eight weeks (ROI 4 mm) (CS/HAp: 39 ± 9.3%; CS/HAp/BMP-2: 45.7 ± 6.6%; CS/HAp/P28: 34.1 ± 6.1%; Collagen sponge: 26.2 ± 2.3%; Collagen sponge/BMP-2: 23.2 ± 3.3%). (**b**) Graph of mean bone mineral density per sample group in the entire defect and margin after eight weeks (ROI 4 mm) (CS/HAp: 449.06 ± 66.69 mg/cm^3; CS/HAp/BMP-2: 497.03 ± 57.45 mg/cm^3; CS/HAp/P28: 438.37 ± 38.94 mg/cm^3; Collagen sponge: 402.6 ± 28.45 mg/cm^3; Collagen sponge/BMP-2: 360.83 ± 22.93 mg/cm^3. Significant difference was achieved in CS/HAp/rhBMP-2 treatments compared to the others. However, the values might be due to traces of HAp, which is a type of ceramic. (* $p < 0.05$).

Previously, the BV/TV values of the nude collagen sponge and collagen sponge soaked with a clinical dose of BMP-2 (5000 ng) were reported to be around only 4% and 9%, respectively [89]. This value was much less than the values recorded in this work, where the newly formulated scaffolds with 100 ng rhBMP-2 yielded more than 40% BV/TV value,

which was almost four times more than the reported BV/TV of collagen sponge/rhBMP-2. This result also validated the efficiency of the growth factor UV grafting method compared to the anionic binding method, where the latter might lead to a burst release phenomenon, thus resulting in a low yield of new bone formation [90]. Furthermore, the report showed decreased BV/TV values in increasing BMP-2 concentrations, indicating decreased bone healing. However, an increased ectopic bone formation was yielded with increasing BMP-2 concentrations in the collagen sponge [89]. Therefore, the low dose of rhBMP-2 and its peptide, P28, in the chitosan-based scaffold might be the better alternative for clinical use.

3.8. Histological Assessment of the Femoral Defects Treated with the Scaffolds

The harvested femoral condyles after eight weeks of healing were embedded in resin blocks and sectioned longitudinally to observe the bone defect in a sagittal view. The overview of the Hematoxylin-Eosin (HE), Von Kossa (VK), Tartrate-Resistant Acid Phosphatase (TRAP), as well as calcein and xylenol fluorochrome labelling, is presented in Figure 10.

HE staining was carried out for a deep qualitative analysis of the tissues according to ISO10993-6:2016 to assess local tissue changes post-implantation of biomedical devices, where the inflammatory response, tissue morphology, presence of fibrosis, necrosis and some more factors were evaluated [91,92]. In the defect implanted with nude CS/HAp, it can be observed that there was inflammation around the scaffold with some multinucleated giant cells, compared to the defects implanted with CS/HAp/rhBMP-2 and CS/HAp/P28, where there was more resorption observed, and the scaffold had broken down, despite the incomplete degradation. While this inflammation remained low, it was suggested that the CS/HAp scaffold was well tolerated and non-toxic. This result matched the absence of clinical signs during the in vivo phase. In addition, non-anastomosed mature bone lamellae were observed in CS/HAp/P28 scaffolds, suggesting that the P28 peptide can upregulate the osteoblast differentiation and lead to the bone regeneration towards the later stage of hard callus remodelled bone formation [93]. This result was in line with previous work investigating P28 peptides in Si/HAp scaffold, where this peptide provided a significant new bone formation and increased osteoblastic activity compared with nude scaffolds and empty defects [38]. Therefore, it can be postulated that there was a sign of bone formation present that could lead to healing in the long run.

Von Kossa staining was used to stain calcium black, thereby distinguishing between osteoid and mature mineralised bone matrix [94,95]. Sections from the nude CS/HAp scaffold showed signs of remodelling that occurred around the defect margin. Defects implanted with CS/HApp28 and CS/HAp BMP treatments resulted in bone islets been formed around the scaffold, and some calcium could be observed. However, this calcium could also have originated from the scaffold composite itself since hydroxyapatite is composed of calcium [96]. Subsequently, the defects implanted with both collagen sponges with and without BMP-2 seemed to be healed since the cortex was completely intact and the trabecular bone had remodelled that it was not distinguishable from the other side.

The presence of osteoclasts, seen as multinucleated cells under the microscope [97], was evaluated in TRAP-stained slides. Only a few osteoclasts were observed in all implanted materials. In scaffold conditions, osteoclasts were present at the edge of newly formed bone tissue inside the defect and the margin. Some osteoclasts were also observed at the edge of residual mineralised material. This result indicates that the implanted scaffolds can recruit TRAP-positive cells, which might be aided by the rough surface of the scaffolds that support cell attachment and proliferation [98]. Nevertheless, the observed osteoclastic activity could suggest that the bony callus stage of the bone healing process was just initiated [97]. Conversely, fewer osteoclasts were seen in the defects implanted with a collagen sponge compared to the scaffold conditions, which was in line with observations from Vao Kossa staining that indicated that healing and remodelling was near completion.
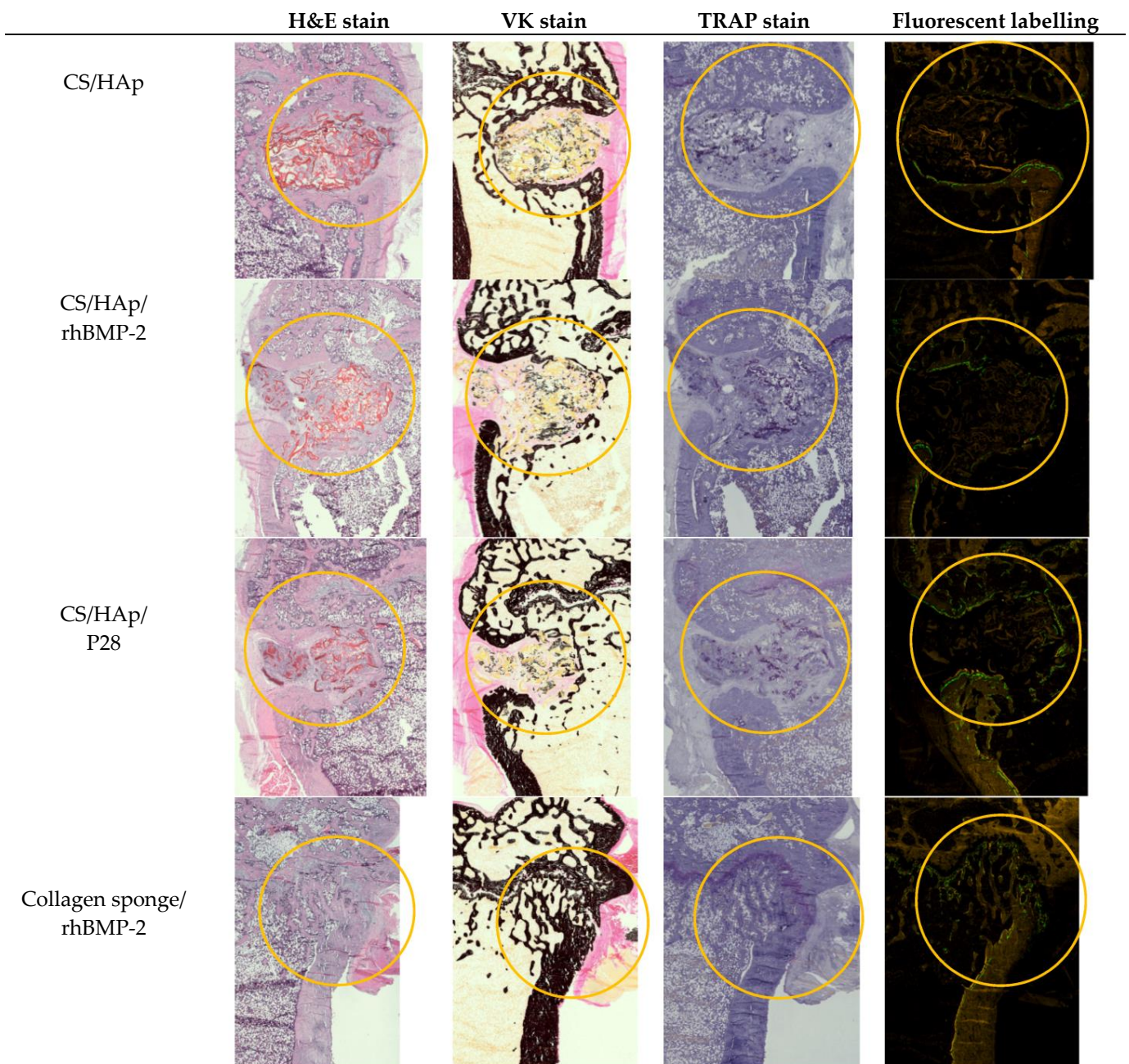
Figure 10. An overview of the HE, VK and TRAP staining as well as the calcein and xylenol fluorescent labelling on the femoral condyles after eight weeks of healing. Observing the defect closure, the CS/HAp/P28 scaffolds presented better bone healing compared to CS/HAp and CS/HAp/rhBMP-2. (Annotation: Yellow circle = Implantation site).

Fluorochrome labelling indicated the uptake of the labelling agent on the day of injection, thus showing that the bone healing process was ongoing during the injection days. It was observed that double labelling was mainly present along the defect margin in chitosan scaffold-implanted samples, suggesting that the physiological bone remodelling cycle was ongoing at the defect margin [99]. Rare double or single labelling was seen at the surface of mineralised tissue inside the defect, leading to the mineralisation process, which occurred at the new-bone tissue or the residual material surface at that specified time point [100,101]. Therefore, the mineralisation was faster inside the defect when present. In collagen sponge conditions, a few fluorochrome labelling were seen at the bone surface and

corresponded only to double labelling suggesting physiological bone remodelling at the bone surface. Double labelling was mainly seen at the bone surface at the defect entrance and was co-localised with osteoid tissue leading to the residual bone formation process at the defect entrance [102].

4. Conclusions

A bone-tissue-mimicking scaffold with osteoinductive growth factors is crucial to treat bone defects. This study presented CS/HAp scaffolds covalently linked with either BMP-2 or its P28 via a UV crosslinking process. ALP activity and ARS-CPC assay were evaluated to validate that our photo-crosslinking fabrication method did not interfere with the functionality of the growth factors. It was recorded that the ALP activity of C2C12 had increased in both BMP-2 and P28 cultures, where 100 μg/mL P28 was comparable to 0.5 μg/mL BMP-2 after two weeks. The C2C12 cultured with CS/HAp/BMP-2 and CS/HAp/P28 scaffolds had also shown an increased ALP activity compared to the negative controls. ARS-CPC assay presented the highest optical density in 0.3 μg/mL BMP-2 and 50 μg/mL P28, while the highest intensity of ARS was observed in C2C12 cultured with CS/HAp/BMP-2 and CS/HAp/P28 scaffolds compared to the negative controls. The in vivo osteogenesis was investigated via rat femoral condyle defect model, where the new bone mineral density and the bone volume were found to increase in all CS/HAp scaffolds after eight weeks compared to the collagen sponges. The histological procedures showed a favourable bone regeneration efficacy through the CS/HAp/P28, thus showing the use of CS/HAp scaffolds with P28 as a promising osteoinductive scaffold for bone healing applications.

Hence, chitosan scaffold with P28 appears to be the alternative to its protein of origin, rhBMP-2, in bone tissue engineering for bone defect healing for its potent osteogenicity and biocompatibility, as well as its non-toxicity features following the implantation in the femoral condyles of the rats. However, due to the insufficient scaffold biodegradability in vivo, improved formulations should be considered to obtain a better degradation profile following implantation.

References

1. Sun, T.; Qu, Y.; Cui, W.; Yang, L.; Ji, Y.; Yu, W.; Navinduth, R.; Shao, Z.; Yang, H.; Guo, X. Evaluation of osteogenic inductivity of a novel BMP2-mimicking peptide P28 and P28-containing bone composite. *J. Biomed. Mater. Res. Part A* **2017**, *106*, 210–220. [CrossRef] [PubMed]

2. Cui, W.; Liu, Q.; Yang, L.; Wang, K.; Sun, T.; Ji, Y.; Liu, L.; Yu, W.; Qu, Y.; Wang, J. Sustained Delivery of BMP-2-Related Peptide from the True Bone Ceramics/Hollow Mesoporous Silica Nanoparticles Scaffold for Bone Tissue Regeneration. *ACS Biomater. Sci. Eng.* **2018**, *4*, 211–221. [CrossRef] [PubMed]

3. Meng, C.; Su, W.; Liu, M.; Yao, S.; Ding, Q.; Yu, K.; Xiong, Z.; Chen, K.; Guo, X.; Bo, L.; et al. Controlled delivery of bone morphogenic protein-2-related peptide from mineralised extracellular matrix-based scaffold induces bone regeneration. *Mater. Sci. Eng. C* **2021**, *126*, 112182. [CrossRef] [PubMed]

4. Sparks, D.S.; Saifzadeh, S.; Savi, F.M.; Dlaska, C.E.; Berner, A.; Henkel, J.; Reichert, J.C.; Wullschleger, M.; Ren, J.; Cipitria, A.; et al. A preclinical large-animal model for the assessment of critical-size load-bearing bone defect reconstruction. *Nat. Protoc.* **2020**, *15*, 877–924. [CrossRef]

5. Klein, A.; Baranowski, A.; Ritz, U.; Mack, C.; Götz, H.; Langendorf, E.; Al-Nawas, B.; Rommens, P.M.; Hofmann, A. Effect of bone sialoprotein coating on progression of bone formation in a femoral defect model in rats. *Eur. J. Trauma Emerg. Surg.* **2019**, *46*, 277–286. [CrossRef]

6. Jahan, K.; Manickam, G.; Tabrizian, M.; Murshed, M. In vitro and in vivo investigation of osteogenic properties of self-contained phosphate-releasing injectable purine-crosslinked chitosan-hydroxyapatite constructs. *Sci. Rep.* **2020**, *10*, 11603. [CrossRef] [PubMed]

7. Zhang, X.; Chen, Y.; Han, J.; Mo, J.; Dong, P.; Zhuo, Y.; Feng, Y. Biocompatiable silk fibroin/carboxymethyl chitosan/strontium substituted hydroxyapatite/cellulose nanocrystal composite scaffolds for bone tissue engineering. *Int. J. Biol. Macromol.* **2019**, *136*, 1247–1257. [CrossRef]

8. Henkel, J. Bone Tissue Engineering in Two Preclinical Ovine Animal Models. Ph.D. Thesis, Queensland University of Technology, Brisbane, Australia, 2017.

9. Taraballi, F.; Bauza, G.; McCulloch, P.; Harris, J.; Tasciotti, E. Concise Review: Biomimetic Functionalization of Biomaterials to Stimulate the Endogenous Healing Process of Cartilage and Bone Tissue. *Tissue Eng. Regen. Med.* **2017**, *6*, 2186–2196. [CrossRef]

10. Burke, G.; Cao, Z.; Devine, D.M.; Major, I. Preparation of biodegradable polyethylene glycol dimethacrylate hydrogels via thiol-ene chemistry. *Polymers* **2019**, *11*, 1339. [CrossRef]

11. Fournet, M.E.B.; Azaman, F.A.; Gunbay, S.; Chen, Y.Y.; Devine, D.M. Orthopedic 3D Printing in Orthopedic Medicine. In *Polymer-Based Additive Manufaturing: Biomedical Application*; Devine, D.M., Ed.; Springer: Cham, Switzerland, 2019; pp. 121–142.

12. Makadia, H.K.; Steven, S.J. Poly Lactic-co-Glycolic Acid (PLGA) as Biodegradable Controlled Drug Delivery Carrier. *Polymers* **2012**, *3*, 1377–1397. [CrossRef]

13. Chen, L.; Liu, J.; Guan, M.; Zhou, T.; Duan, X.; Xiang, Z. Growth factor and its polymer scaffold-based delivery system for cartilage tissue engineering. *Int. J. Nanomed.* **2020**, *15*, 6097–6111. [CrossRef]

14. Azaman, F.A.; Zhou, K.; Blanes-Martínez, M.M.; Fournet, M.B.; Devine, D.M. Bioresorbable Chitosan-Based Bone Regeneration Scaffold Using Various Bioceramics and the Alteration of Photoinitiator Concentration in an Extended UV Photocrosslinking Reaction. *Gels* **2022**, *8*, 696. [CrossRef]

15. Sukpaita, T.; Chirachanchai, S.; Suwattanachai, P.; Everts, V.; Pimkhaokham, A.; Ampornaramveth, R.S. In vivo bone regeneration induced by a Scaffold of chitosan/dicarboxylic acid seeded with human periodontal ligament cells. *Int. J. Mol. Sci.* **2019**, *20*, 4883. [CrossRef] [PubMed]

16. Maji, K.; Dasgupta, S.; Pramanik, K.; Bissoyi, A. Preparation and Evaluation of Gelatin-Chitosan-Nanobioglass 3D Porous Scaffold for Bone Tissue Engineering. *Int. J. Biomater.* **2016**, *2016*, 9825659. [CrossRef] [PubMed]

17. Chang, F.C.; Tsao, C.T.; Lin, A.; Zhang, M.; Levengood, S.; Zhang, M. PEG-Chitosan Hydrogel with Tunable Stiffness for Study of Drug Response of Breast Cancer Cells. *Polymers* **2016**, *8*, 112. [CrossRef] [PubMed]

18. Fourie, J.; Taute, F.; du Preez, L.; de Beer, D. Chitosan Composite Biomaterials for Bone Tissue Engineering—A Review. *Regen. Eng. Transl. Med.* **2022**, *8*, 1–21. [CrossRef]

19. Marques, C.; Som, C.; Schmutz, M.; Borges, O.; Borchard, G. How the Lack of Chitosan Characterization Precludes Implementation of the Safe-by-Design Concept. *Front. Bioeng. Biotechnol.* **2020**, *8*, 165. [CrossRef]

20. Kumar, A.; Kumar, A. Chitosan as a biomedical material: Properties and applications. In *Biopolymers: Structure, Performance and Applications*; Mishra, A.K., Hussain, C.M., Mishra, S.B., Eds.; Nova Science Publishers, Inc.: New York, NY, USA, 2017; pp. 139–154.

21. Venkatesan, J.; Kim, S.K. Chitosan composites for bone tissue engineering—An overview. *Mar. Drugs* **2010**, *8*, 2252–2266. [CrossRef]

22. Zhang, F.; King, M.W. Biodegradable Polymers as the Pivotal Player in the Design of Tissue Engineering Scaffolds. *Adv. Healthc. Mater.* **2020**, *9*, 1901358. [CrossRef]

23. Jhala, D.; Rather, H.A.; Vasita, R. Extracellular matrix mimicking polycaprolactone-chitosan nanofibers promote stemness maintenance of mesenchymal stem cells via spheroid formation. *Biomed. Mater.* **2020**, *15*, 035011. [CrossRef]

24. Nicolas, J.; Magli, S.; Rabbachin, L.; Sampaolesi, S.; Nicotra, F.; Russo, L. 3D Extracellular Matrix Mimics: Fundamental Concepts and Role of Materials Chemistry to Influence Stem Cell Fate. *Biomacromolecules* **2020**, *21*, 1968–1994. [CrossRef] [PubMed]

25. Rodriguez-Barroso, L.G.; Azaman, F.A.; Pogue, R.; Devine, D.; Fournet, M.B. Monitoring In Vitro Extracellular Matrix Protein Conformations in the Presence of Biomimetic Bone-Regeneration Scaffolds Using Functionalized Gold-Edge-Coated Triangular Silver Nanoparticles. *Nanomaterials* **2022**, *13*, 57. [CrossRef] [PubMed]

26. Maachou, H.; Bal, K.E.; Bal, Y.; Chagnes, A.; Cote, G.; Alliouche, D. Characterization and in vitro bioactivity of chitosan/hydroxyapatite composite membrane prepared by freeze-gelation method. *Trends Biomater. Artif. Organs* **2008**, *22*, 15–24.

27. Li, B.; Wang, J.; Moustafa, M.E.; Yang, H. Ecofriendly Method to Dissolve Chitosan in Plain Water. *ACS Biomater. Sci. Eng.* **2019**, *5*, 6355–6360. [CrossRef]

28. Zheng, X.; Yin, Y.; Jiang, W.; Xing, L.; Pu, J. Low-mass chitosan. *BioResources* **2015**, *10*, 2338–2349.

29. Reves, B.T.; Jennings, J.A.; Bumgardner, J.D.; Haggard, W.O. Osteoinductivity assessment of BMP-2 loaded composite chitosan-nano-hydroxyapatite scaffolds in a rat muscle pouch. *Materials* **2011**, *4*, 1360–1374. [CrossRef]

30. Bjelić, D.; Finšgar, M. The role of growth factors in bioactive coatings. *Pharmaceutics* **2021**, *13*, 1083. [CrossRef]

31. El Bialy, I.; Jiskoot, W.; Reza Nejadnik, M. Formulation, Delivery and Stability of Bone Morphogenetic Proteins for Effective Bone Regeneration. *Pharm. Res.* **2017**, *34*, 1152–1170. [CrossRef]

32. Devine, D.M.; Hoctor, E.; Hayes, J.S.; Sheehan, E.; Evans, C.H. Extended release of proteins following encapsulation in hydroxyapatite/chitosan composite scaffolds for bone tissue engineering applications. *Mater. Sci. Eng. C* **2018**, *84*, 281–289. [CrossRef]

33. Bullock, G.; Atkinson, J.; Gentile, P.; Hatton, P.; Miller, C. Osteogenic peptides and attachment methods determine tissue regeneration in modified bone graft substitutes. *J. Funct. Biomater.* **2021**, *12*, 22. [CrossRef]

34. Alves, A.; Wancket, L.; Metz, A. Current considerations in medical device pathology. In *Biocompatibility and Performance of Medical Devices*, 2nd ed.; Elsevier Ltd.: Amsterdam, The Netherlands, 2020; pp. 491–543.

35. Rosenberg, M.; Shilo, D.; Galperin, L.; Capucha, T.; Tarabieh, K.; Rachmiel, A.; Segal, E. Bone morphogenic protein 2-loaded porous silicon carriers for osteoinductive implants. *Pharmaceutics* **2019**, *11*, 602. [CrossRef] [PubMed]

36. Zhao, G.; Zhang, L.; Che, L.; Li, H.; Liu, Y.; Fang, J. Revisiting bone morphogenetic protein-2 knuckle epitope and redesigning the epitope-derived peptides. *J. Pept. Sci.* **2021**, *27*, e3309. [CrossRef] [PubMed]

37. Wu, Y.; Jia, G.; Chi, H.; Jiao, Z.; Sun, Y. Integrated In Silico-In Vitro Identification and Optimization of Bone Morphogenic Protein-2 Armpit Epitope as Its Antagonist Binding Site. *Protein J.* **2020**, *39*, 703–710. [CrossRef] [PubMed]

38. Cui, W.; Sun, G.; Qu, Y.; Xiong, Y.; Sun, T.; Ji, Y.; Yang, L.; Shao, Z.; Ma, J.; Zhang, S.; et al. Repair of rat calvarial defects using Si-doped hydroxyapatite scaffolds loaded with a bone morphogenetic protein-2-related peptide. *J. Orthop. Res.* **2016**, *34*, 1874–1882. [CrossRef]

39. Bain, J.L.; Bonvallet, P.P.; Abou-Arraj, R.V.; Schupbach, P.; Reddy, M.S.; Bellis, S.L. Enhancement of the Regenerative Potential of Anorganic Bovine Bone Graft Utilising a Polyglutamate-Modified BMP2 Peptide with Improved Binding to Calcium-Containing Materials. *Tissue Eng. Part A* **2015**, *17–18*, 2426–2436. [CrossRef]

40. De Gorter, D.J.J.; Van Dinther, M.; Ten Dijke, P. *Measurement of Constitutive Activity of BMP Type I Receptors*, 1st ed.; Elsevier Inc.: Amsterdam, The Netherlands, 2010; Volume 484.

41. Hidaka, Y.; Chiba-ohkuma, R.; Karakida, T.; Onuma, K. Combined Effect of Midazolam and Bone Morphogenetic Protein-2 for Differentiation Induction from C2C12 Myoblast Cells to Osteoblasts. *Pharmaceutics* **2020**, *12*, 218. [CrossRef]

42. Blackwood, K.A.; Bock, N.; Dargaville, T.R.; Ann Woodruff, M. Scaffolds for growth factor delivery as applied to bone tissue engineering. *Int. J. Polym. Sci.* **2012**, *2012*, 174942. [CrossRef]

43. Katagiri, T.; Yamaguchi, A.; Komaki, M.; Abe, E.; Takahashi, N.; Ikeda, T.; Rosen, V.; Wozney, J.M.; Fujisawa-Sehara, A.; Suda, T. Bone morphogenetic protein-2 converts the differentiation pathway of C2C12 myoblasts into the osteoblast lineage. *J. Cell Biol.* **1994**, *127*, 1755–1766. [CrossRef]

44. Kelly, F. Evaluation of Modified Flow-Through Pulsed UV Technology for Bacterial Inactivation with Comparison to a Standard Continuous-Flow Low Pressure UV System. Ph.D. Thesis, National University of Ireland Galway, Galway, Ireland, 2019.

45. Becerra, J.; Rodriguez, M.; Leal, D.; Noris-Suarez, K.; Gonzalez, G. Chitosan-collagen-hydroxyapatite membranes for tissue engineering. *J. Mater. Sci. Mater. Med.* **2022**, *33*, 18. [CrossRef]

46. Mohiuddin, O.A.; Campbell, B.; Poche, J.N.; Ma, M.; Rogers, E.; Gaupp, D.; Harrison, M.A.A.; Bunnell, B.A.; Hayes, D.J.; Gimble, J.M. Decellularized Adipose Tissue Hydrogel Promotes Bone Regeneration in Critical-Sized Mouse Femoral Defect Model. *Front. Bioeng. Biotechnol.* **2019**, *7*, 211. [CrossRef]

47. van Gaalen, S.M.; Kruyt, M.C.; Geuze, R.E.; de Bruijn, J.D.; Alblas, J.; Dhert, W.J.A. Use of fluorochrome labels in in vivo bone tissue engineering research. *Tissue Eng. Part B. Rev.* **2010**, *16*, 209–217. [CrossRef] [PubMed]

48. Porter, A.; Irwin, R.; Miller, J.; Horan, D.J.; Robling, A.G.; McCabe, L.R. Quick and inexpensive paraffin-embedding method for dynamic bone formation analyses. *Sci. Rep.* **2017**, *7*, 42505. [CrossRef]

49. Liao, Y.; Li, H.; Shu, R.; Chen, H.; Zhao, L.; Song, Z.; Zhou, W. Mesoporous Hydroxyapatite/Chitosan Loaded with Recombinant-Human Amelogenin Could Enhance Antibacterial Effect and Promote Periodontal Regeneration. *Front. Cell. Infect. Microbiol.* **2020**, *10*, 180. [CrossRef] [PubMed]

50. Fern, H.W.; Salimi, M.N. Hydroxyapatite nanoparticles produced by direct precipitation method: Optimisation and characterisation studies. *AIP Conf. Proc.* **2021**, *2339*, 020215.

51. Nazeer, M.A.; Yilgör, E.; Yilgör, I. Intercalated chitosan/hydroxyapatite nanocomposites: Promising materials for bone tissue engineering applications. *Carbohydr. Polym.* **2017**, *175*, 38–46. [CrossRef]

52. Predoi, D.; Iconaru, S.L.; Predoi, M.V.; Stan, G.E.; Buton, N. Synthesis, characterisation, and antimicrobial activity of magnesium-doped hydroxyapatite suspensions. *Nanomaterials* **2019**, *9*, 1295. [CrossRef] [PubMed]

53. Shemshad, S.; Kamali, S.; Khavandi, A.; Azari, S. Synthesis, characterisation and in-vitro behavior of natural chitosan-hydroxyapatite-diopside nanocomposite scaffold for bone tissue engineering. *Int. J. Polym. Mater. Polym. Biomater.* **2019**, *68*, 516–526. [CrossRef]

54. Halloran, D.; Vrathasha, V.; Durbano, H.W.; Nohe, A. Bone morphogenetic protein-2 conjugated to quantum dot®s is biologically functional. *Nanomaterials* **2020**, *10*, 1208. [CrossRef]

55. Anesi, A.; Di Bartolomeo, M.; Pellacani, A.; Ferretti, M.; Cavani, F.; Salvatori, R.; Nocini, R.; Palumbo, C.; Chiarini, L. Bone Healing Evaluation Following Different Osteotomic Techniques in Animal Models: A Suitable Method for Clinical Insights. *Appl. Sci.* **2020**, *10*, 7165. [CrossRef]

56. Sun, T.; Liu, M.; Yao, S.; Ji, Y.; Shi, L.; Tang, K.; Xiong, Z.; Yang, F.; Chen, K.; Guo, X. Guided osteoporotic bone regeneration with composite scaffolds of mineralised ECM/heparin membrane loaded with BMP2-related peptide. *Int. J. Nanomed.* **2018**, *13*, 791–804. [CrossRef]

57. Xiong, Z.; Cui, W.; Sun, T.; Teng, Y.; Qu, Y.; Yang, L.; Zhou, J.; Chen, K.; Yao, S.; Shao, Z.; et al. Sustained delivery of PlGF-2123-144-fused BMP2-related peptide P28 from small intestinal submucosa/polylactic acid scaffold material for bone tissue regeneration. *RSC Adv.* **2020**, *10*, 7289–7300. [CrossRef] [PubMed]

58. Zhou, J.; Xiong, Z.; Liu, M.; Yang, L.; Yao, S.; Chen, K.; Yu, K.; Qu, Y.; Sun, T.; Guo, X. Creation of bony microenvironment with extracellular matrix doped-bioactive ceramics to enhance osteoblast behavior and delivery of aspartic acid-modified bmp-2 peptides. *Int. J. Nanomed.* **2020**, *15*, 8465–8478. [CrossRef]

59. Honda, T.; Yamamoto, H.; Ishii, A.; Inui, M. PDZRN3 Negatively Regulates BMP-2–induced Osteoblast Differentiation through Inhibition of Wnt Signaling. *Mol. Biol. Cell* **2010**, *21*, 3269–3277. [CrossRef] [PubMed]

60. Saito, A.; Suzuki, Y.; Ogata, S.I.; Ohtsuki, C.; Tanihara, M. Activation of osteo-progenitor cells by a novel synthetic peptide derived from the bone morphogenetic protein-2 knuckle epitope. *Biochim. Biophys. Acta Proteins Proteom.* **2003**, *1651*, 60–67. [CrossRef]

61. Gudivada, V.N.; Huang, C.J.; Luo, Y.H.; Dong, G.C. A cyclic bmp-2 peptide upregulates bmp-2 protein-induced cell signaling in myogenic cells. *Polymers* **2021**, *13*, 2549. [CrossRef] [PubMed]

62. Wu, Y.; Zhou, J.; Li, Y.; Zhou, Y.; Cui, Y.; Yang, G.; Hong, Y. Rap1A regulates osteoblastic differentiation via the ERK and p38 mediated signaling. *PLoS ONE* **2015**, *10*, e0143777. [CrossRef]

63. Metzger, S. Tunable and Cell-Responsive 3D poly(ethylene glycol) Microenvironments for the Development of Tissue Models. Ph.D. Thesis, University of Zurich, Zurich, Switzerland, 2016.

64. Sondag, G.R.; Salihoglu, S.; Lababidi, S.L.; Crowder, D.C.; Moussa, F.M.; Abdelmagid, S.M.; Safadi, F.F. Osteoactivin induces transdifferentiation of C2C12 myoblasts into osteoblasts. *J. Cell. Physiol.* **2014**, *229*, 955–966. [CrossRef]

65. Kang, Q.; Sun, M.H.; Cheng, H.; Peng, Y.; Montag, A.G.; Deyrup, A.T.; Jiang, W.; Luu, H.H.; Luo, J.; Szatkowski, J.P.; et al. Characterisation of the distinct orthotopic bone-forming activity of 14 BMPs using recombinant adenovirus-mediated gene delivery. *Gene Ther.* **2004**, *11*, 1312–1320. [CrossRef]

66. Akiyama, S.; Katagiri, T.; Namiki, M.; Yamaji, N.; Yamamoto, N.; Miyama, K.; Shibuya, H.; Ueno, N.; Wozney, J.M.; Suda, T. Constitutively active BMP type I receptors transduce BMP-2 signals without the ligand in C2C12 myoblasts. *Exp. Cell Res.* **1997**, *235*, 362–369. [CrossRef]

67. Rauch, C.; Brunet, A.C.; Deleule, J.; Farge, E. C2C12 myoblast/osteoblast transdifferentiation steps enhanced by epigenetic inhibition of BMP2 endocytosis C2C12 myoblast/osteoblast transdifferentiation steps enhanced by epigenetic inhibition of BMP2 endocytosis. *Am. J. Physiol. Cell Physiol.* **2002**, *283*, 235–243. [CrossRef]

68. Lin, D.P.L.; Carnagarin, R.; Dharmarajan, A.; Dass, C.R. Transdifferentiation of myoblasts into osteoblasts—Possible use for bone therapy. *J. Pharm. Pharmacol.* **2017**, *69*, 1661–1671. [CrossRef] [PubMed]

69. Gleeson, J.P.; Plunkett, N.A.; O'Brien, F.J. Addition of hydroxyapatite improves stiffness, interconnectivity and osteogenic potential of a highly porous collagen-based scaffold for bone tissue regeneration. *Eur. Cells Mater.* **2010**, *20*, 218–230. [CrossRef] [PubMed]

70. Song, R.; Wang, D.; Zeng, R.; Wang, J. Synergistic effects of fibroblast growth factor-2 and bone morphogenetic protein-2 on bone induction. *Mol. Med. Rep.* **2017**, *16*, 4483–4492. [CrossRef] [PubMed]

71. Ho, M.H.; Liao, M.H.; Lin, Y.L.; Lai, C.H.; Lin, P.I.; Chen, R.M. Improving effects of chitosan nanofiber scaffolds on osteoblast proliferation and maturation. *Int. J. Nanomed.* **2014**, *9*, 4293–4304.

72. Shalumon, K.T.; Sheu, C.; Fong, Y.T.; Liao, H.T.; Chen, J.P. Microsphere-based hierarchically juxtapositioned biphasic scaffolds prepared frompoly(lactic-co-glycolic acid) and nanohydroxyapatite for osteochondral tissue engineering. *Polymers* **2016**, *8*, 429. [CrossRef] [PubMed]

73. Kisiel, M. Bone Enhancement with BMP-2 for Safe Clinical Translation. Ph.D. Thesis, Uppsala University, Uppsala, Sweden, 2013.

74. Bouyer, M.; Guillot, R.; Lavaud, J.; Plettinx, C.; Olivier, C.; Curry, V.; Boutonnat, J.; Coll, J.L.; Peyrin, F.; Josserand, V.; et al. Surface delivery of tunable doses of BMP-2 from an adaptable polymeric scaffold induces volumetric bone regeneration. *Biomaterials* **2016**, *104*, 168–181. [CrossRef] [PubMed]

75. Lee, D.; Wufuer, M.; Kim, I.; Choi, T.H.; Kim, B.J.; Jung, H.G.; Jeon, B.; Lee, G.; Jeon, O.H.; Chang, H.; et al. Sequential dual-drug delivery of BMP-2 and alendronate from hydroxyapatite-collagen scaffolds for enhanced bone regeneration. *Sci. Rep.* **2021**, *11*, 746. [CrossRef]

76. Hettiaratchi, M.H.; Krishnan, L.; Rouse, T.; Chou, C.; McDevitt, T.C.; Guldberg, R.E. Heparin-mediated delivery of bone morphogenetic protein-2 improves spatial localisation of bone regeneration. *Sci. Adv.* **2020**, *6*, eaay1240. [CrossRef]

77. Mumcuoglu, D.; Fahmy-Garcia, S.; Ridwan, Y.; Nickel, J.; Farrell, E.; Kluijtmans, S.G.J.M.; van Osch, G.J.V.M. Injectable BMP-2 delivery system based on collagen-derived microspheres and alginate induced bone formation in a time-and dose-dependent manner. *Eur. Cells Mater.* **2018**, *35*, 242–254. [CrossRef]

78. Durham, E.L.; Kishinchand, R.; Grey, Z.J.; Cray, J.J. rhBMP2 alone does not induce macrophage polarisation towards an increased inflammatory response. *Mol. Immunol.* **2020**, *117*, 94–100. [CrossRef]

79. Alghamdi, H.S.; Van Den Beucken, J.J.J.P.; Jansen, J.A. Osteoporotic rat models for evaluation of osseointegration of bone implants. *Tissue Eng. Part C Methods* **2014**, *20*, 493–505. [CrossRef] [PubMed]

80. Luckanagul, J.A.; Metavarayuth, K.; Feng, S.; Maneesaay, P.; Clark, A.Y.; Yang, X.; García, A.J.; Wang, Q. Tobacco Mosaic Virus Functionalized Alginate Hydrogel Scaffolds for Bone Regeneration in Rats with Cranial Defect. *ACS Biomater. Sci. Eng.* **2016**, *2*, 606–615. [CrossRef] [PubMed]

81. Brennan, M.P.; Sinusas, A.J.; Horvath, T.L.; Collins, J.G.; Harding, M.J. Correlation between body weight changes and postoperative pain in rats treated with meloxicam or buprenorphine. *Lab Anim.* **2009**, *38*, 87–93. [CrossRef] [PubMed]

82. Baker, E.A. Enhancing Osseointegration of Orthopaedic Implants with Titania Nanotube Surfaces. Ph.D. Thesis, Michigan Technological University, Houghton, MI, USA, 2016.

83. Zhao, Z.; Yang, D.; Ma, X.; Zhao, H.; Nie, C.; Si, Z. Successful repair of a critical-sized bone defect in the rat femur with a newly developed external fixator. *Tohoku J. Exp. Med.* **2009**, *219*, 115–120. [CrossRef]

84. Zhang, H.Y.; Liu, Q.; Liu, J.Q.; Wang, J.; Yang, H.X.; Xu, X.J.; Xie, M.J.; Liu, X.D.; Yu, S.B.; Zhang, M.; et al. Molecular changes in peripheral blood involving osteoarthritic joint remodelling. *J. Oral Rehabil.* **2019**, *46*, 820–827. [CrossRef]

85. Zhang, J.; Liao, L.; Zhu, J.; Wan, X.; Xie, M.; Zhang, H.; Zhang, M.; Lu, L.; Yang, H.; Jing, D.; et al. Osteochondral Interface Stiffening in Mandibular Condylar Osteoarthritis. *J. Dent. Res.* **2018**, *97*, 563–570. [CrossRef]

86. Bejar, J.; Peled, E.; Boss, J.H. Vasculature deprivation-Induced osteonecrosis of the rat femoral head as a model for therapeutic trials. *Theor. Biol. Med. Model.* **2005**, *2*, 24. [CrossRef]

87. Chen, X.; Zhou, R.; Chen, B.; Chen, J. Nanohydroxyapatite/cellulose nanocrystals/silk fibroin ternary scaffolds for rat calvarial defect regeneration. *RSC Adv.* **2016**, *6*, 35684–35691. [CrossRef]

88. Lyles, M.B.; Hu, J.C.; Varanasi, V.G.; Hollinger, J.O.; Athanasiou, K.A. Bone tissue engineering. *Regen. Eng. Musculoskelet. Tissues Interfaces* **2015**, *1*, 97–134.

89. Durham, E.L.; Nicole Howie, R.; Hall, S.R.; Larson, N.; Oakes, B.; Houck, R.; Grey, Z.; Steed, M.; LaRue, A.C.; Muise-Helmericks, R.; et al. Optimising bone wound healing using BMP2 with absorbable collagen sponge and Talymed nanofiber scaffold. *J. Transl. Med.* **2018**, *16*, 321. [CrossRef]

90. Oliveira, É.R.; Nie, L.; Podstawczyk, D.; Allahbakhsh, A.; Ratnayake, J.; Brasil, D.L.; Shavandi, A. Advances in growth factor delivery for bone tissue engineering. *Int. J. Mol. Sci.* **2021**, *22*, 903. [CrossRef] [PubMed]

91. Maglio, M.; Salamanna, F.; Brogini, S.; Borsari, V.; Pagani, S.; Nicoli Aldini, N.; Giavaresi, G.; Fini, M. Histological, Histomorphometrical, and Biomechanical Studies of Bone-Implanted Medical Devices: Hard Resin Embedding. *Biomed Res. Int.* **2020**, *2020*, 1804630. [CrossRef]

92. Ansari, M. Bone tissue regeneration: Biology, strategies and interface studies. *Prog. Biomater.* **2019**, *8*, 223–237. [CrossRef] [PubMed]

93. Li, J.; Stocum, D.L. Fracture Healing. In *Basic and Applied Bone Biology*; Burr, D.B., Allen, M.R., Eds.; Elsevier Science Publishing Co., Inc.: Amsterdam, The Netherlands, 2014; pp. 205–223.

94. Gruber, H.E.; Ingram, J.A. Basic Staining and Histochemical Techniques and Immunohistochemical Localizations Using Bone Sections. In *Handbook of Histology Methods for Bone and Cartilage*, 1st ed.; An, Y.H., Martin, K.L., Eds.; Humana Press: Totowa, NJ, USA, 2003; pp. 281–286.

95. de Azevedo e Sousa Munhoz, M.; Torres Pomini, K.; de Guzzi Plepis, A.M.; da Conceiç̧ão Amaro Martins, V.; Machado, E.G.; de Moraes, R. Elastin-derived scaffolding associated or not with bone morphogenetic protein (BMP) or hydroxyapatite (HA) in the repair process of metaphyseal bone defects. *PLoS ONE* **2020**, *15*, e0231112.

96. Bin Sulaiman, S.; Keong, T.K.; Cheng, C.H.; Bin Saim, A.; Hj Idrus, R.B. Tricalcium phosphate/hydroxyapatite (TCP-HA) bone scaffold as potential candidate for the formation of tissue engineered bone. *Indian J. Med. Res.* **2013**, *137*, 1093–1101.

97. Chen, X.; Zhao, Y.; Geng, S.; Miron, R.J.; Zhang, Q.; Wu, C.; Zhang, Y. In vivo experimental study on bone regeneration in critical bone defects using PIB nanogels/boron-containing mesoporous bioactive glass composite scaffold. *Int. J. Nanomed.* **2015**, *10*, 839–846.

98. e Silva, E.P.; Huang, B.; Helaehil, J.V.; Nalesso, P.R.L.; Bagne, L.; de Oliveira, M.A.; Albiazetti, G.C.C.; Aldalbahi, A.; El-Newehy, M.; Santamaria, M.; et al. In vivo study of conductive 3D printed PCL/MWCNTs scaffolds with electrical stimulation for bone tissue engineering. *Bio-Design Manuf.* **2021**, *4*, 190–202. [CrossRef]

99. Erben, R.G. Bone-Labeling Techniques. In *Handbook of Histology Methods for Bone and Cartilage*, 1st ed.; An, Y.H., Martin, K.L., Eds.; Humana Press: Totowa, NJ, USA, 2003; pp. 99–117.

100. Shim, M.-J. Bone Changes in Femoral Bone of Mice Using Calcein Labeling. *Korean J. Clin. Lab. Sci.* **2016**, *48*, 114–117. [CrossRef]

101. Goldschlager, T.; Abdelkader, A.; Kerr, J.; Boundy, I.; Jenkin, G. Undecalcified bone preparation for histology, histomorphometry and fluorochrome analysis. *J. Vis. Exp.* **2010**, *35*, e1707.

102. Xiao, C.; Zhou, H.; Liu, G.; Zhang, P.; Fu, Y.; Hou, H.; Tang, T.; Fan, X. Bone marrow stromal cells with a combined expression of BMP-2 and VEGF-165 enhanced bone regeneration. *Biomed. Mater.* **2011**, *6*, 015013. [CrossRef]